JGR Atmospheres

RESEARCH ARTICLE
10.1029/2024JD041258

Unraveling Ice Nucleating Particle Concentration Variability: Insights Into Source Emissions Origin and Parameterizations

A. Canzi[1], E. Freney[1], P. Grzegorczyk[1], J. L. Baray[1], L. Lacher[2], and C. Planche[1,3]

[1]Laboratoire de Météorologie Physique, INSU-CNRS UMR, Université Clermont-Auvergne, Clermont-Ferrand, France, [2]Institute of Meteorology and Climate Research, Atmospheric Aerosol Research (IMKAAF), Karlsruhe Institute of Technology (KIT), Karlsruhe, Germany, [3]Institut Universitaire de France (IUF), Paris, France

Key Points:

- Short lived dust events have significant influences on atmospheric ice nucleating particles concentrations
- Accounting for air mass characteristics offers valuable insights into the temporal variability of atmospheric ice nucleating particles concentrations
- Polluted air masses are frequently associated with elevated concentrations of ice nucleating particles

Correspondence to:
E. Freney and C. Planche,
evelyn.freney@uca.fr;
celine.planche@uca.fr

Citation:
Canzi, A., Freney, E., Grzegorczyk, P., Baray, J. L., Lacher, L., & Planche, C. (2025). Unraveling ice nucleating particle concentration variability: Insights into source emissions origin and parameterizations. *Journal of Geophysical Research: Atmospheres*, *130*, e2024JD041258. https://doi.org/10.1029/2024JD041258

Received 28 MAR 2024
Accepted 7 APR 2025

Author Contribution:
Writing – review & editing: L. Lacher

Abstract Despite having very low atmospheric concentrations, ice-nucleating particles (INPs) play an important role in the formation of atmospheric ice crystals at temperatures warmer than −35°C and hence in the atmospheric precipitation cycle. Moreover, they tend to have a very high spatiotemporal variability. In order to understand this variability, long-term measurements with high temporal resolution are essential. This paper presents an analysis of 3 months of online INP measurements (10 min time-resolved), using a PINE cloud chamber (−33°C ≤ T ≤ −22°C). Measurements were made from December 2022 to March 2023 at the PUY station (France, 1,465 m a.s.l), a site exposed to a variety of air masses including free troposphere conditions. A large part of the temporal variability of INP concentrations (over four orders of magnitude at a single temperature) can be explained by air mass origin. INP concentrations measured for oceanic air masses are in the lower range (from ≈0.1 to ≈10 L^{-1}). Those for continental air masses are in a medium range (from ≈1 to ≈100 L^{-1}) and depend on the level of pollution of the air mass. INP concentrations measured for southern air masses show highest concentrations (from ≈10 to ≈500 L^{-1}) and mostly depend on the amount of dust in the ambient air. Moreover, measurements were conducted during two dust events revealing INP concentrations over 1000 L^{-1} at −32°C. Subsequently, a set of parameterizations capable of tracing the measured INP variability were developed. This will facilitate our understanding of the impact of INP concentrations on mixed-phase cloud properties with cloud models.

Plain Language Summary Ice Nucleating Particles (INP) are responsible for primary ice formation at temperatures warmer than −35℃ and thus can have a strong influence on mixed-phase cloud properties. Only a small fraction of aerosol particles can act as INPs. The ice nucleation (IN) ability of aerosol particles depends on their physicochemical properties and environmental temperature. This work shows how the INP concentrations are different according to origins of air masses. We present an analysis of 3 months of continuous measurements in winter 2023 at the PUY station (France, 1,465 m a.s.l) conducted with online IN chamber. Hence, a set of parameterizations is developed according to specific environments sampled during the campaign (oceanic, continental clean and polluted, Saharan dust).

1. Introduction

Ice-nucleating particles (INPs) enable ice formation in clouds under both ambient ice and water-saturated conditions at temperatures above −35°C (Pruppacher & Klett, 1997). These particles significantly influence cloud properties such as ice water content, precipitation rate, cloud lifetime, and radiative properties, thereby impacting the climate system (Fan et al., 2017; Muhlbauer & Lohmann, 2009; Tan & Storelvmo, 2016). Despite their importance, accurately representing the role of INPs in climate models remains a challenge due to insufficient observational data and the complex, poorly understood processes involved in aerosol-cloud interactions (Burrows et al., 2022).

INPs represent a very small fraction of total aerosol particles (≈10^{-5} at −30°C), making them challenging to quantify (Cziczo et al., 2017). Their atmospheric concentration also varies significantly over time and location, by more than four orders of magnitude at a single temperature. This variability results from differences in the ice nucleation ability of particles based on their physicochemical properties, which depend on the origin of emission sources (Kanji et al., 2017). Therefore, INP concentrations at a specific location are influenced not only by local emissions but also by the transport of air masses from their source regions (Lacher et al., 2021).

Ice heterogeneous nucleation occurs when ice forms with the help of an aerosol particles (INP) and can occur via different processes. Deposition nucleation occurs when water vapor turns directly into ice on a surface without becoming liquid first. This deposition mode is known to be relevant for cirrus cloud regime (Hoose & Möhler, 2012; Kanji et al., 2017) and therefore mainly occurs at lower temperature than those considered in this work. Condensation freezing happens when supercooled water condenses on a surface and freezes at the same time. Immersion freezing occurs when a particle inside supercooled water triggers ice formation as the temperature drops. Finally, contact freezing takes place when a particle touches a supercooled droplet and causes it to freeze. Condensation and immersion freezing modes are often associated because both occur at humidity level above water saturation, making them difficult to distinguish. The condensation/immersion freezing mode is thought to be the most important in the mixed-phase cloud regime (Prenni et al., 2009). It is therefore the one on which this study focuses.

The primary sources of INPs globally are arid regions such as deserts, through dust emissions (Kanji et al., 2017; Vergara-Temprado et al., 2017), and the ocean, through sea spray emissions. Marine environments typically produce lower INP concentrations than terrestrial ones, and can exhibit INP concentrations that are dominated by nearby terrestrial sources rather than local marine ones (DeMott et al., 2016; Mason et al., 2015; McCluskey et al., 2018; Vergara-Temprado et al., 2018). Conversely, desert dust particles have high ice-nucleating potential at temperature below −20°C (DeMott et al., 2015; Möhler et al., 2006; Niemand et al., 2012) due to their mineral composition and large sizes. Biological aerosol particles have also been identified as efficient INPs in several different environments (Bras et al., 2024; Creamean et al., 2013; Schneider et al., 2021). Other contributors to the global INP population include continental environments, where biomass burning (Jahn et al., 2020; Levin et al., 2016), soil dust (Suski et al., 2018), and anthropogenic emissions play significant roles. Zhao et al. (2019) and Ren et al. (2023) observed a positive correlation between pollution levels in continental air masses and the ice-nucleating potential of aerosol particles in the immersion freezing mode, indicating that polluted environments can contain substantial amounts of INPs. To accurately represent the potential impact of this variability on cloud properties, it is beneficial for cloud scale models to incorporate parameterizations based on long-term atmospheric measurements.

Several methods exist to measure INPs (e.g., DeMott et al., 2011). These methods typically have unique measurable freezing temperatures and water/ice saturation conditions, allowing for complementary assessments of various ice nucleation modes (Vali et al., 2015). Offline methods provide INP concentrations based on the collection of particles onto filters with a time resolution ranging from a few hours to several days, for temperatures between 0°C and −30°C (Lacher et al., 2024). Online methods, such as ice nucleation chambers (Möhler et al., 2021; Rogers, 1993), provide INP concentrations by cooling air samples, with a time resolution of a few minutes. However, due their low detection limit, these instruments are typically only able to determine ambient INP concentrations at temperatures lower than −20°C. Intercomparison campaigns between different methods performed under ambient air conditions (DeMott et al., 2017; Lacher et al., 2024) have shown good agreement between similar measurement methods (either online and offline) when conducted under the same operating conditions with good temporal overlap. However, discrepancies of up to a factor of five have been observed between instruments, due to variable operating conditions, filter technologies, and inlet losses under certain atmospheric conditions. This suggests that comparing measurements from various sites can be biased when different instruments and conditions are used. To address these challenges, it is important to characterize the effect of the environment from a single site exposed to various influences using a single method that can be applied at other remote locations for future comparisons. In this context, a 3 months INP measurement campaign is conducted at the Puy de Dôme (PUY) station (1,465 m a.s.l.). PUY is an ideal location for long-term INP concentration measurements for two primary reasons. First, the station is influenced by a diverse range of air masses: oceanic air from the west, continental air from the northeast, and southern air containing large amounts of Saharan dust (Deguillaume et al., 2014). Second, during winter, the station often lies within the free troposphere (Baray et al., 2020; Farah et al., 2018, 2021; Freney et al., 2016), where cloud formation occurs.

Previously reported INP measurements are used to develop ice nucleation parametrizations that can be implemented into global and mesoscale models. Existing parametrizations follow two different approaches: stochastic (time dependent) and deterministic. Deterministic parameterizations are expressing INP concentration as a

function of temperature (T) and/or ice supersaturation (S_i) (e.g., Steinke et al., 2015), and sometimes of an additional parameter describing aerosols properties. Deterministic models are more frequently used in cloud models, as it is easier to implement and computationally less expensive. The advantage of single-parameter based parameterizations (e.g., Meyers et al., 1992) is that they provide a simple way to express heterogeneous ice nucleation, making their implementation in most mesoscale models relatively straightforward. Two-parameters based parameterizations (Chen et al., 2024; DeMott et al., 2010, 2015; Niemand et al., 2012; Phillips et al., 2008) are also integrating a parameter based on aerosol physical properties (e.g., aerosols larger than 500 nm and total surface concentration). They represent a step forward into the representation on aerosol cloud interaction for heterogeneous ice nucleation (Burrows et al., 2022; Planche et al., 2015). A large number of composition-resolved parameterizations also exit, for example, for organic carbon content (Trueblood et al., 2021; Wilson et al., 2015), which can be implemented in models if an aerosol and chemistry module is used (e.g., Mann et al., 2010; Planche et al., 2017).

Mesoscale models such as WRF (Skamarock et al., 2008) and Méso-NH (Lac et al., 2018) use deterministic approach to represent heterogeneous ice nucleation process. Bulk microphysics schemes (e.g., Keita et al., 2019; Milbrandt & Yau, 2005; Vié et al., 2016) and bin microphysical cloud schemes (e.g., DESCAM; Flossmann & Wobrock, 2010; Planche et al., 2010, 2014) are widely used in modeling ice nucleation. For deposition and condensation freezing modes, the approach developed by Meyers et al. (1992) is commonly applied. Immersion freezing is typically described using the formulation introduced by Bigg (1953). The major drawback of these parameterizations is that they do not consider aerosol properties. Furthermore, they have been developed on a limited number of observations and are suitable for one type of environment only. Therefore, they cannot account for the variability of N_{INP} observed in the atmosphere at a single temperature.

This work presents online INP measurements in the temperature range of −22°C and −33°C in the condensation/immersion freezing mode, complementary to previous measurements at the site using offline measurements (Bras et al., 2024). The online cloud chamber (Möhler et al., 2021) has the added advantage of operating in a fully autonomously manner. This method measures INP concentrations with a 10 min time resolution, allowing the assessment of the relationship between INP abundance and air mass type. The air mass type is defined by a classification based on the analysis of back-trajectories of measured air masses during the whole campaign. Since the goal is to evaluate the impact of air mass type on cloud properties over Western Europe using cloud-scale models. A set of parameterizations, suitable to cloud-scale models is proposed. These parameterizations are capable of representing INP concentration for each air mass type.

2. Methodology

2.1. Site Description

The Puy de Dôme station (PUY, 45°77' N, 2°96' E, and 1,465 m above sea level) is located at the highest point of the Chaîne des Puys, a north-south-oriented volcanic mountain range in central France. PUY is recognized as a global atmospheric monitoring station (GAW) and is also part of the Aerosol, Clouds, and Trace Gases Research Infrastructure (ACTRIS) and Integrated Carbon Observation System (ICOS) European research infrastructures. Detailed information about the history, scientific context, national and international structuration, and technical description of the observation systems can be found in Baray et al. (2020). This site is known for its exposure to long-range air masses originating from both continental and oceanic regions, making it a valuable location for atmospheric studies (Baray et al., 2020; Farah et al., 2018). Due to its altitude and geographical surroundings, PUY is near the boundary between the mixing layer and the free troposphere providing an excellent opportunity to investigate different atmospheric layers (Farah et al., 2018; Freney et al., 2016), and, in the case of this study, the ice nucleation properties of aerosol particles.

At this site, a large suite of instruments continuously monitor meteorological parameters such as temperature (T), humidity (RH), and pressure (P), as well as a diverse array of online and offline measurement techniques to analyze the in situ chemical and physical properties of gases and aerosol particles (Baray et al., 2020).

2.2. INP Measurements

The measurement of INP concentration (N_{INP}) is conducted using the PINE-c chamber (Portable Ice Nucleation Experiment commercial, PINE-05-01; Bilfinger Noell GmbH) connected to the whole air inlet of PUY (50%

cutoff at 30 μm; Willeke and Baron (2005)). Ambient aerosol particles sampled through the inlet are passively dried to approximately 40% RH_w before being sampled by the different instruments. In the PINE, aerosol particles are further dried after passing through a nafion dryer. More details of the operational principle of this cloud chamber is provided in Möhler et al. (2021). The specificity of PINE chamber is that the cooling and saturation leading to INP activation are achieved through the pressure reduction (0.15 bar) of a sample of ambient air within the chamber, thereby replicating the nucleation process in clouds upon air mass lifting. Measurements are performed at water saturation conditions ($100\% < RH_w < 102\%$) involving the prior activation of aerosol particles in droplets and thus characterizing the condensation/immersion freezing mode. The identification and counting of activated particles (droplets and crystals with optical diameters between 0.7 and 220 μm) are done with an Optical Particle Counter (OPC; fidas-pine; Palas GmbH) at the chamber outlet. Ice crystals, whose optical diameters are larger than other particles, can be distinguished from droplets by setting a threshold on the optical size. The threshold value is calculated for every run. Each run consists of the succession of three modes: flush mode when ambient air circulates in the chamber, expansion mode when a pressure reduction and simultaneous gas temperature cooling in the PINE vessel is performed, and refill mode when the chamber is refilled with filtered ambient air up to initial pressure condition. The flush mode is performed at a flow rate of 2 L min^{-1} during 450 s, ensuring that the sampled air mass is exchanged in the vessel. The expansion mode is performed at a flow rate of 3 L min^{-1} down to a pressure of approximately 700 mbar. The refill mode is performed at a flow rate of 2 L min^{-1} to ambient pressure (≈850 mbar at PUY). Each run lasts approximately 10 min.

The effective volume measured for each run is approximately 2 L, which implies that the detection limit for INP concentration in a single run is 0.5 INP L^{-1} (i.e., 1 particle/PINE sampling volume). To measure concentrations lower than this value, multiple runs under the same sampling conditions and time-averaging of the obtained N_{INP} over a prolonged period are necessary. The measurement protocol involves wall temperature ramps allowing for a scan of the temperature range in 2 hours. The gas temperature in the PINE vessel quickly equilibrates to the wall temperature prior to the expansion experiment. During the expansion, the gas temperature evolution does not follow the adiabatic mode as it continues to exchange temperature with the walls. The gas temperature inside the chamber is cooled by 7°C during the expansion cycle. The considered temperature for the measurement is the minimum gas temperature reached at the bottom of the chamber, at the end of expansion step. The target for this temperature is between −22°C and −33°C. PINE is capable of performing measurements at temperatures higher than −20°C. However, due to the very low INP concentrations in this temperature range, it requires a specific protocol with multiple consecutive runs performed at the same temperature, and increased flush duration. All the data provided are for standard temperature and pressure (STP) conditions. To process the raw data, we used the PIA (PINE INP Analysis) software that calculates INP concentrations, temperature spectra, and overview plots (https://codebase.helmholtz.cloud/pine/pia_software). All data are quality controlled using SaQC (Lennart Schmidt et al., 2023).

The working principle of PINE is different from that of other ice nucleation chambers such as HINC-Auto (Brunner & Kanji, 2021), HINC (Lacher et al., 2017), and the most well-known being the CSU-CFDC (Rogers et al., 2001). In CSU-CFDC, the activation of aerosols is obtained by the circulation in a laminar air flow between two walls in supersaturated conditions. The supersaturation can be controlled by adjusting the temperature difference between the walls. Activated crystals are then detected downstream to the chamber with an OPC, as for PINE.

This sampling period ran from 15 December 2022 to 19 March 2023, excluding 4 days in (22–25) February and 4 days in (11–14) March due to power outages, resulting in 87 days of measurements, and a total of 11,869 measurement runs. Additionally, background measurements were made regularly (at least once a week) during several hours (total of 1,419 runs). These background measurements involve operating the instrument through a series of runs with an aerosol filter at the inlet. Background runs aim to verify the validity of the measurements and detect potential icing of the chamber. Wilbourn et al. (2024) demonstrated that artifacts may occur in measurements at temperatures warmer than −20°C under certain operating conditions. The analysis of these background measurements did not reveal any anomalies that would suggest chamber icing or non-conformity in the results.

2.3. Other Measurements and Numerical Tools

Total particle concentration (N_{AP}) in the size range 10 nm up to 3 μm was measured with a Condensation Particle Counter (CPC, TSI 3010). A Multi-Angle Absorption Photometer (MAAP; Petzold & Schönlinner, 2004; Petzold et al., 2005) was also in operation during the whole period, providing equivalent black carbon (BC) mass

concentration (M_{BC}). These instruments have been described in detail in a number of publications (Farah et al., 2018, 2021; Freney et al., 2011, 2016).

COPLid is a high-power lidar in operation at the Cézeaux (CZ) site located 11 km west of PUY, and at an altitude of 420 m. It has operated continuously from 2009 to 2022 in a single wavelength configuration (355 nm) including polarized and Raman channels (Baray et al., 2020; Fréville et al., 2015). It was upgraded to a multi-wavelength configuration (355, 532, and 1,064 nm) in October 2022. In the present study, we measured vertical profiles of volume backscatter coefficients, extinction coefficients, and depolarization ratios with a temporal resolution of 10 min, in order to determine the height of the dust plume and acquire a vertical profile of dust concentration during the Saharan dust events.

Mineral dust particles, particularly those from arid regions like deserts, can act as efficient INPs and significantly increase N_{INP} in the atmosphere. Some papers (Boose et al., 2016; Brunner et al., 2021) have reported an increase in INP concentrations at temperatures below −20°C by a factor of 10–100, attributed to long-range dust transport from the Saharan desert. Furthermore, the chemical composition of dust particles can vary widely depending on their source, leading to variations in their ice nucleation activity (Kanji et al., 2017). Therefore, to account for the variability of INP concentrations during the campaign based on the origin of the air masses, it is essential to quantify dust mass concentration (M_{DUST}) at any given time during the study period. For this purpose, we used the ENSEMBLE outputs from the Copernicus Atmosphere Monitoring Service (CAMS) (Marécal et al., 2015). CAMS is a service implemented by the ECMWF that provides regional air quality data through a collective of 11 advanced numerical air quality models developed in Europe. These models conduct daily assessments of surface-level pollutants, including M_{DUST}, by assimilating 1 day observational data with the model results. The assessments produced by all 11 models are aggregated to calculate the median value of individual outputs, currently regarded as the most accurate estimate from the ENSEMBLE. The horizontal resolution of the models is $0.1° \times 0.1°$ (approx. 10 km^2) and the temporal resolution is 1 hr. The vertical coverage extends from surface level to 5,000 m a.g.l, divided into 10 non-equidistant levels. For our analyses, we used the ENSEMBLE outputs for M_{DUST} provided for the nearest grid point to PUY and interpolated vertically to its altitude (1,465 m a.s.l).

A list of instrumentation and models used for this paper can be found in Table A1 in Appendix A. The time series of N_{INP}, M_{BC}, and M_{DUST} over the entire duration of the campaign, as well as the origin of the sampled air masses are plotted in Figure A1.

2.4. Air Mass Classification

The ice nucleation properties of aerosol particles depend on their physical and chemical properties (size, chemical composition), and therefore on their origin. Since the measurements of N_{INP} are conducted in ambient air, it is essential to identify the origin of the sampled air masses to distinguish them (Deguillaume et al., 2014; Venzac et al., 2009). The identification of the origin of air mass based on back trajectory calculations using the CAT (Computing Atmospheric Trajectory tool) model which is described in Baray et al. (2020). CAT provides a group of 45 back-trajectories, automatically calculated every hour, from the PUY location with a temporal resolution of 15 min. Back-trajectories are calculated using ECMWF ERA5 wind data at a spatial resolution of 0.5°, a temporal resolution of 3 hr, on 23 pressure levels distributed non-linearly between 1,000 hPa and 200 hPa. The topography matrix is at a resolution of 10 km (Bezděk & Sebera, 2013). CAT provides the altitude of the air mass and the estimated planetary boundary layer (PBL) height interpolated at every trajectory point. Back trajectories are computed from 45 starting points. The exact location of the inlet, plus eight points (±0.1° lon/lat) at five different levels (over 50 m) to take into account of orographic effect at PUY. Figure 1a represents the density of the back-trajectories over a 0.5° grid for the studied period resulting in a total of $2,280 \times 45$ back-trajectories (since 2,280 and 45 correspond to the total duration (in hours) and the number of back-trajectories per hour, respectively). During the studied period, CAT estimates that the station is within the PBL (BL height, BLH, at PUY >1,400 m) 55% of the time, whatever the air mass origin, which is consistent with previous studies conducted during winter conditions (Baray et al., 2020; Farah et al., 2018).

The classification of air masses based on their origin, is determined by the time spent on different directional sectors (West, South, and North + East; called hereafter W-sec, S-sec, and NE-sec, respectively) during the 72 hr before their arrival at PUY (Figure 1a). The impact of precipitation is not considered in the back trajectory analysis. The assigned category corresponds to the sector where the air mass has spent the longest time. W-sec contains mainly air masses originating from over the Atlantic Ocean, and accounts for 52% of the total air mass

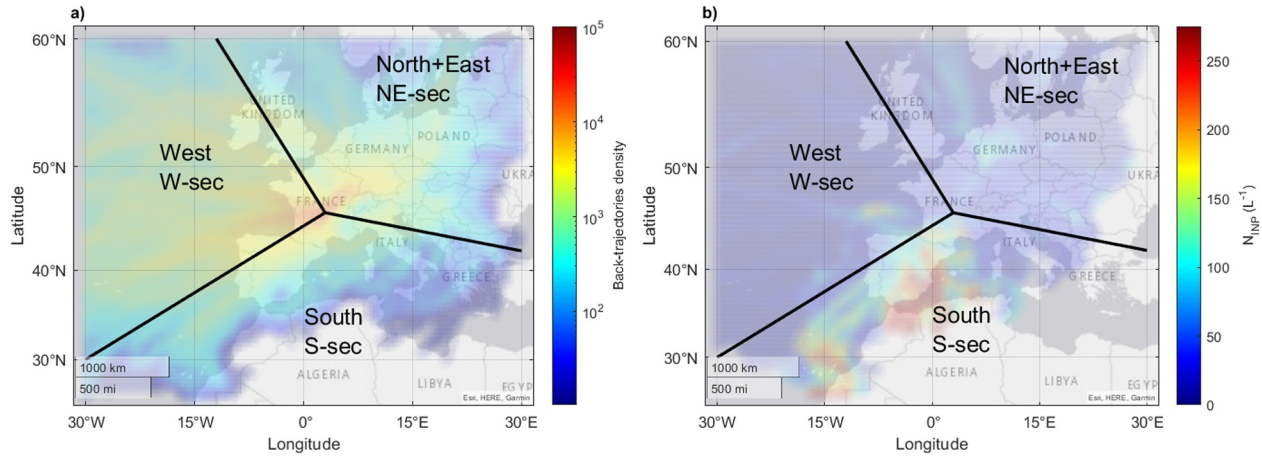

Figure 1. Geographical analysis (over a 0.5° grid) of the 72hr back-trajectories performed using CAT model during the campaign period (from 15 December 2022 to 19 March 2023). Panel (a) gives the back-trajectories density obtained (i.e., 2,280 × 45 back-trajectories), and Panel (b) represents the INP concentration measured at −32°C at PUY associated to each back trajectory and averaged over a 0.5° grid.

sources (Table 1). These westerly air masses are characterized by high humidity levels and make up a substantial proportion of cloudy conditions observed at PUY (Baray et al., 2019). In fact, 55% of the W-sec measurements are taken under cloudy conditions (ambient $RH_w > 99.9\%$). The NE-sec encompasses air masses, which represents 28% of the total sampled air mass sources, mainly originating from continental regions and 95% of the associated measurements were conducted under clear sky conditions. Lastly, the S-sec represents the remaining 20%, with a majority of measurements (81%) taken under clear sky conditions. The W-sec air masses predominantly pass an average of 76% (24%) of their time over the ocean (land), that is, marine (continental) ratio in Table 1, and they spent 18% of the time within the marine boundary layer (BL). On the other hand, the S-sec air masses combine marine and continental influences almost equally on average, spending 4% of time in BL (i.e., marine or continental). Lastly, the NE-sec air masses primarily come from the continent (78% on average) and spend 8% of their time in the continental BL. All these data are summarized in Table 1.

3. Observations/Results

Figure 2 depicts N_{INP} measured at PUY during the campaign, as well as measurements from other studies carried out with PINE in different location. The dataset includes measurements from Möhler et al. (2021), collected at the Southern Great Plains (SGP) site over 45 consecutive days from 1 October to 15 November 2019. It also incorporates data from Wilbourn et al. (2024), gathered at the Eastern North Atlantic Ocean (ENA) site between 1 October and 30 November 2021. A detailed comparative analysis of measurements at SGP and ENA is provided by Wilbourn et al. (2024). The SGP site is located in Oklahoma (USA) where the influence is mostly continental whereas the ENA site which is located in the Azores have a strong marine influence. One important difference between these two sites and PUY is that the measurements conducted at SGP and ENA are taken at ground level (5 m a.g.l) thereby in the boundary layer at all times, and likely more influenced by local sources. Figure 2 also includes INP concentration measured by Bras et al. (2024) using an offline method. Those measurement were collected at PUY from 7 November 2018 to 25 May 2019.

At PUY, the 1°C bin averaged N_{INP} over the whole period varies from 20 L^{-1} at −30°C, to 1.2 L^{-1} at −22°C (Figure 2a). The average values are close to those measured at ENA and lower than that of SGP (64 L^{-1} at −30°C, 6 L^{-1} at −22°C). The variability of observed N_{INP} at PUY is much greater than at ENA and SGP. For a given temperature, 6 hr averaged N_{INP} spans roughly three orders of magnitude while it stays below two orders of magnitudes for the two other sites. The larger diversity of air masses observed at PUY and by the significant amount of measurement taken under free tropospheric conditions (45%) can explain this difference. This is illustrated by the median values depicted in Figure 2b showing that the averaged N_{INP} measured at PUY are influenced by the high concentrations of southern air masses loaded with desert dust. At warmer temperatures, there is a significant part (>50% at PUY at T = −22°C) of zero N_{INP} measured. These zero values are integrated

Table 1
Distribution of the Sampled Air Masses at PUY According to Their Origin

Sector	Marine ratio	Continental ratio	Marine BL ratio	Continental BL ratio	Total ratio
West (W-sec)	76%	24%	18%	2.4%	52%
South (S-sec)	45%	55%	4%	4%	20%
North + East (NE-sec)	22%	78%	6%	8%	28%

Note. The West (W-sec), South (S-sec), and North + East (NE-sec) sectors are defined in Figure 1. For each sector, the percentage indicates the averaged fraction of time spent over seas (marine ratio) or over lands (continental ratio) for the 72 hr back-trajectories of each sector. Marine (or Continental) BL ratio represents the fraction of time spent in BL while the air mass was traveling over seas (or lands). Total ratio is the proportion of air masses coming from each sector over the total.

into the calculation of average values. A figure depicting the fraction of zero values measured as a function of temperature as well of the size of each bin is available in Appendix A (Figure A2).

We note that even there is no overlap with the temperature range of measurements conducted by Bras et al. (2024), the dependence on temperature seems to have a consistent behavior in the range of −30°C to −10°C, when comparing to data from the SGP (Möhler et al., 2021). We also notice that the relative position between the different campaigns is the same at all the temperature ranges.

Finally it is worth to notice that no diurnal cycle has been observed during the measurement period. This is consistent with Bras et al. (2024) and Lacher et al. (2024), who reported the absence of day/night contrast at PUY during Weekly Ice Nuclei Samples (WINS) campaign and Puy de Dôme Ice Nucleation Intercomparison Campaign (PICNIC), respectively.

Figure 1b depicts N_{INP} averaged on a 0.5° grid according to back-trajectories. To create this figure, we assume that N_{INP} is conserved throughout the back trajectory. Even though this assumption is not necessarily accurate, it allows to provide an overview of the INP concentration based on geographic origin. Thus air masses originating from North Africa, particularly after passing over Morocco and the Atlas Mountains (S-sec, longitude from 0° to 20°W), are highly concentrated in INPs, while those coming from the Atlantic Ocean and the eastern Mediterranean Sea, on the contrary, present low values of N_{INP} (Figure 1b). Air masses from NE-sec have intermediate

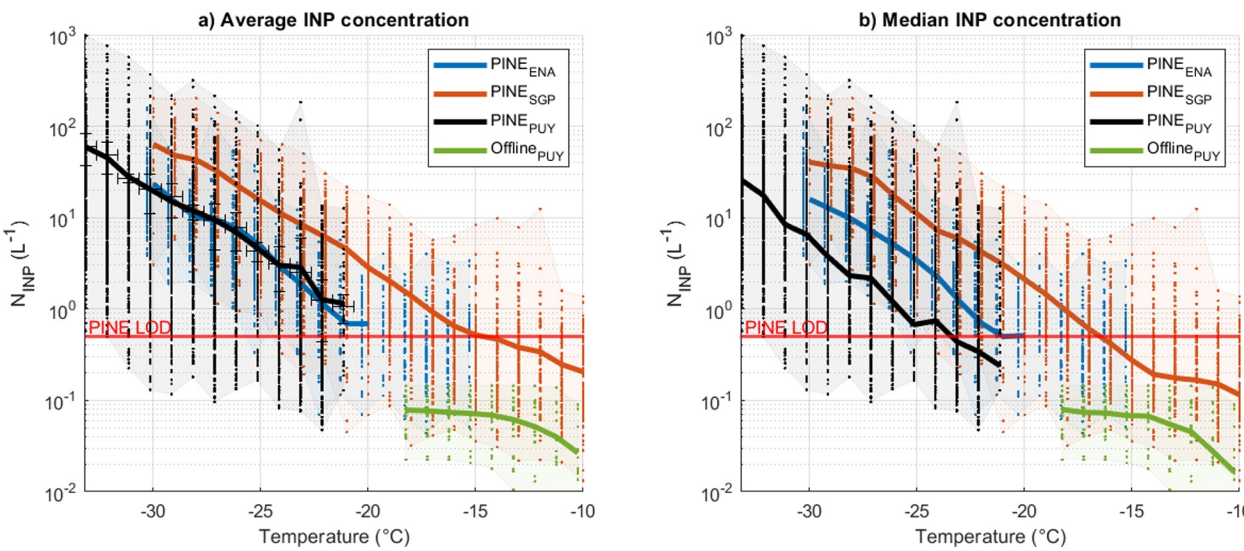

Figure 2. (a) Black line represents average INP concentration as a function of temperature measured with PINE at PUY throughout the entire campaign (87 days; from 15 December 2022 to 19 March 2023). Measurements were taken above liquid water saturation. All data have been averaged within 1°C temperature bin from −33°C to −21°C. Each single dot represents a 6 hr averaged value. Vertical error bars represent the average standard deviation over 6 hr while horizontal error bars indicate the temperature bin size. The shaded area encompasses all 6 hr averaged values. Orange line and dots represent data from Möhler et al. (2021) measured with PINE at SGP. Blue line and dots represents data from Wilbourn et al. (2024) measured with PINE at ENA. Green line and dots represents data from Bras et al. (2024) measured with offline protocol LINDA at PUY, and (b) same as for panel (a) with thick lines representing median values instead of average. Red line shows PINE's limit of detection from a single expansion on both panels.

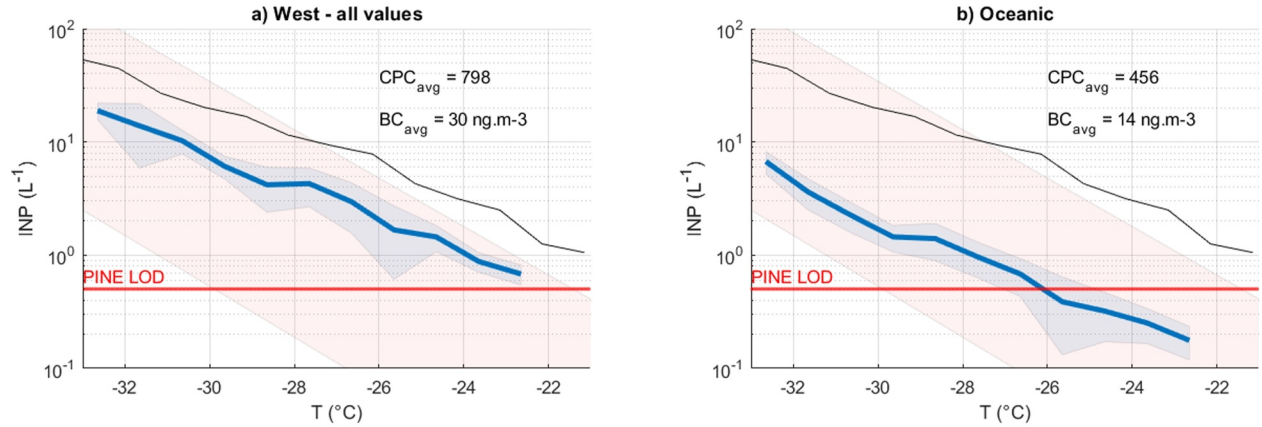

Figure 3. (a) INP averaged concentration as a function of temperature measured with PINE at the PUY station (thick blue lines) for W-sec, and (b) representing an "oceanic" environment. The thin black line represents the average value over the entire campaign (equivalent to the black line in Figure 2a). The shaded blue area represent the 95% confidence interval. The shaded red area represent the range of values reported by DeMott et al. (2016). Red line shows PINE's limit of detection from a single expansion on both panels.

values. Air masses originating from Germany are, on average, more concentrated in INPs. For W-sec, occurrences of high concentrations in the Bay of Biscay are a result of a dust event during which the dust plume crossed a portion of the ocean before reaching PUY. This is in accordance with CAMS outputs (https://atmosphere.copernicus.eu/cams-monitors-first-saharan-dust-episodes-europe-2023).

As N_{INP} at PUY appears to strongly depend on the origin of air masses and thus, on the composition of the particles they carry, the following sections will focus on analyzing INP properties as a function of air mass origin. This is illustrated by Figure A1, which shows the time series of N_{INP}, M_{BC}, and M_{DUST} over the entire duration of the campaign, as well as the origin of the sampled air masses. In this approach, we do not account for local sources of emissions because they cannot be traced by the back-trajectories. These emissions may affect the ice nucleation activity measured at PUY. However, there are several reasons indicating that, in our case, these local sources can be neglected. It was previously demonstrated (Bras et al., 2024), through the comparison of heated and non-heated samples, that the local contribution to ice nucleation activity at PUY is biogenic and that this contribution becomes negligible at temperatures below −18°C. Furthermore, in this study, the measurements are conducted in winter when local biological activity is minimal and when the station more often lies in the residual layer or free troposphere.

For the analyses presented hereafter, we use the INP concentration values measured with a temporal resolution of 10 min. No time-averaging method have been used. All other variables (N_{AP}, M_{BC}, M_{DUST}) are interpolated to the timestamp of INP measurement. For back trajectory analysis, we use the closest in time. As the time resolution is 1 hr, the time difference between back trajectory analysis and INP measurement is always below 30 min.

Two Saharan dust events occurred over Europe on 16–17 February, and then on 22–23 February (called Dust Event #1 or #2 (DuEv#1 or DuEv#2) in Section 4). These short-time events can have a significant impact on N_{INP}, as shown in previous studies (DeMott et al., 2015; Möhler et al., 2006; Niemand et al., 2012). In this work, measurements taken during the two dust events are separated from the main dataset (Section 3.1, 3.2, 3.3) and are discussed separately as a case study period in Section 4.

3.1. Focus on West Sector (W-Sec)

Figure 3a shows the average INP concentration as a function of temperature for W-sec (number of data points (n) = 5,565) excluding measurements done during DuEv#1 and DuEv#2. All INP concentrations taken for air masses originating from W-sec were pooled in temperature bins and averaged with 1°C temperature bin resolution. N_{INP} for W-sec are, on average, 2.5 times lower than those measured across all sectors. The average total particle number concentration (N_{AP}, measured by CPC) and BC mass content are 798 cm^{-3} ($\pm\sigma$ = 1,230 cm^{-3}) and 30 ng m^{-3} ($\pm\sigma$ = 44 ng m^{-3}), respectively.

We focus here on air masses with an oceanic signature, for which mixing with continental sources and aging since leaving the marine environment is minimal. Then, from the back-trajectories of W-sec, we apply the following criteria on $\text{Marine}_{\text{ratio}}$ and continental BL_{ratio} (defined in Section 2.4) in order to be representative of "oceanic" air masses.

- $\text{Marine}_{\text{ratio}} > 80\%$: the air mass spent over 80% of its time over the ocean in the 72 hr preceding the measurement;
- Continental $\text{BL}_{\text{ratio}} < 2\%$: the air mass spent less than 2% of its time in the continental boundary layer in the 72 hr preceding the measurement.

According to this analysis procedure, the "oceanic" air masses spent on average 87% of their time over the ocean, including 28% within the marine BL ($n = 1{,}532$). The associated N_{INP} is, on average, 4 times lower than those of W-sec. Thus, the "oceanic" values (1 L^{-1} at −28°C; see Figure 3b) are in agreement with measurements taken in purely marine environments, which vary between 0.1 and 3 L^{-1} at −28°C (DeMott et al., 2016; Mason et al., 2015; McCluskey et al., 2018; Vergara-Temprado et al., 2018). Also, N_{AP} and M_{BC} observed for these "oceanic" air masses (456 cm^{-3} $\pm\sigma = 393$ cm^{-3}, and 14 ng m^{-3} $\pm\sigma = 22$ ng m^{-3}) are approximately 2 times lower than those of W-sec. It is also worth mentioning that a significant fraction of the INP data points obtained during oceanic air masses are below the LOD of PINE.

Hence, even though PUY is not close to the sea (approximately 300 km from the Atlantic coast), oceanic influences are frequently observed in atmospheric measurements, due to the absence of mountain between the Atlantic coast and PUY (Deguillaume et al., 2014). Applying specific criteria to air mass classification yields reliable N_{INP} for marine/coastal environments. This is particularly adapted in winter when photochemical reactions are minimal.

In order to get closer to remote oceanic conditions, we applied an additional criteria on M_{BC} (<10 ng m^{-3}) which halves the INP concentrations but also drastically reduces the number of samples ($n = 870$). Thus, to obtain more robust results about the chosen criteria to characterize remote oceanic conditions at the PUY station, additional ongoing continuous measurements are necessary.

3.2. Focus on North + East Sector (NE-Sec)

Figure 4a shows the average N_{INP} as a function of temperature considering all measurements made during air masses originating from NE-sec ($n = 1{,}074$), whereas Figures 4b and 4c present how INP properties depend highly on the time spent in BL. To avoid a local pollution influence, our analyses consider only measurements taken when the station (1,465 m a.s.l) lies in free troposphere or residual BL (i.e., BLH <1,400 m a.s.l in CAT outputs; see Section 2.4). On average, N_{INP} measured in NE-sec are 37% lower than the average measured across all sectors. The average N_{AP} measured is 1,151 cm^{-3} ($\pm\sigma = 637$ cm^{-3}) while the average BC content is 159 ng m^{-3} ($\pm\sigma = 141$ ng m^{-3}).

Using the 72 hr back-trajectories, two different categories of air masses are distinguished based on the residence time in BL: for the first one, BL_{ratio} is lower than 1% ($n = 580$; Figure 4b), whereas, for the second one, BL_{ratio} is higher than 20% ($n = 77$; Figure 4c). These two categories represent air masses from continental free troposphere or planetary boundary layer, respectively, and highlight the contrasted properties according to the air mass origin within the NE-sec. In this way, N_{INP} is on average 40% lower or 70% higher than for the average NE-sec, N_{AP} is 913 cm^{-3} ($\pm\sigma = 598$ cm^{-3}) or 1,977 cm^{-3} ($\pm\sigma = 550$ cm^{-3}), and BC content is 81 ng m^{-3} ($\pm\sigma = 107$ ng m^{-3}) or 247 ng m^{-3} ($\pm\sigma = 118$ ng m^{-3}), respectively.

We also observe a strong correlation between N_{INP} and M_{BC} ($R^2 = 0.62$, Pearson p-value $p < 0.001$ at −31°C). Although, BC particles are generally not considered to be efficient INPs in immersion freezing mode and at temperatures above −35°C (Hoose & Möhler, 2012; Kanji et al., 2020; Mahrt et al., 2018, 2023). Some studies (Zhao et al. (2019); Ren et al. (2023)) have reported increased INP activity in polluted air masses, whereas others (Bi et al., 2019; Chen et al., 2018) also reported that showed that no clear correlation between pollution and N_{INP} were observed. Although, BC particles are unlikely to be efficient INP at the PUY, we consider that it is a good tracer for anthropogenically influenced air masses. BC is generally unreactive and unless rainfall occurred during the air mass trajectory, it is relatively long lived. It serves as an indicator of the level of air pollution in the considered air masses. We defined then two categories called "continental clean" ($n = 480$, average residence time in PBL = 2%) and "continental polluted" ($n = 204$, average residence time in PBL = 12%), for which M_{BC} is

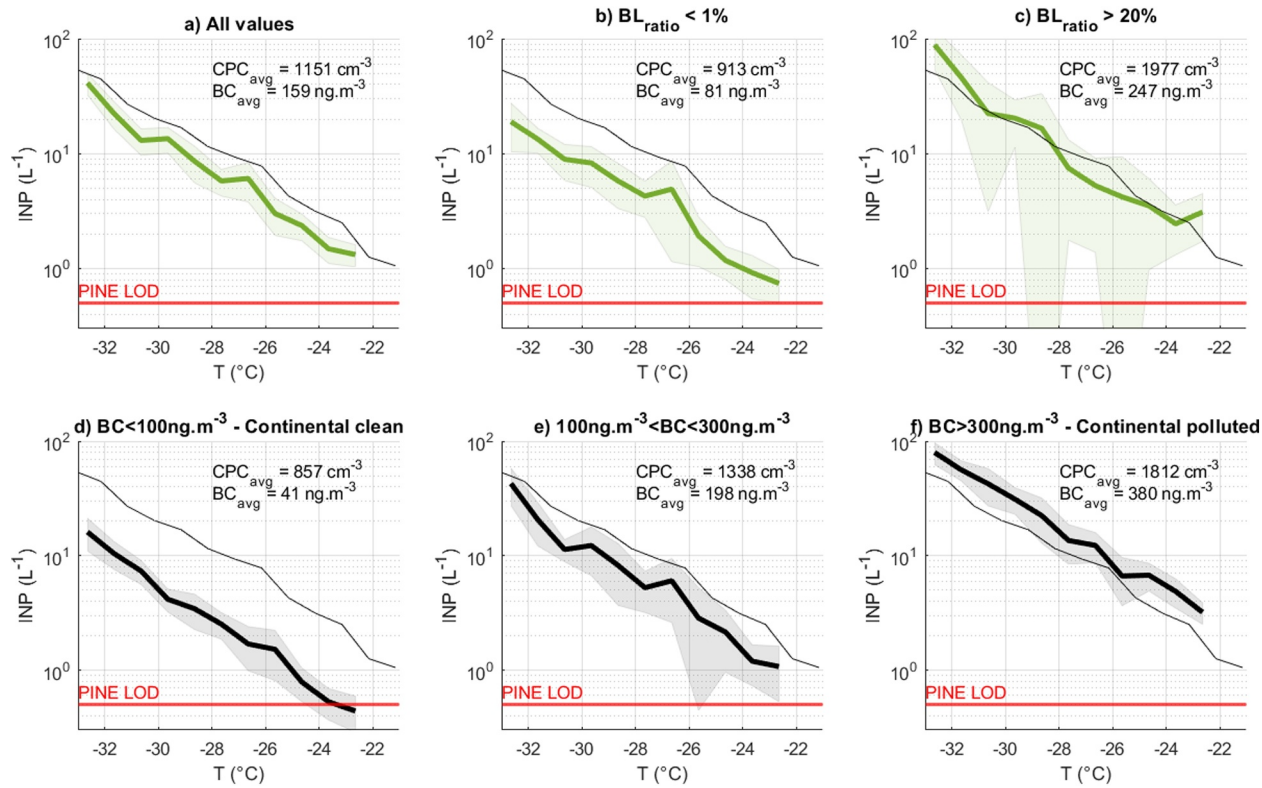

Figure 4. (a) INP averaged concentration as a function of temperature measured with PINE at PUY (thick lines) for the North + East sector (NE-sec), (b) for air masses that spent less than 1% of their time in the boundary layer ($BL_{ratio} < 1\%$), (c) for air masses that spent more than 20% of their time in the boundary layer ($BL_{ratio} > 20\%$), (d) for BC content <100 ng m^{-3}, (e) for BC content between 100 and 200 ng m^{-3}, and (f) for BC content >300 ng m^{-3}. The thin black lines on all panels represent the average value over the entire campaign while the shaded areas represent the 95% confidence interval.

respectively lower than 100 ng m^{-3} and higher than 300 ng m^{-3}. These threshold values correspond respectively to clean rural environments, and to polluted rural and urban environments (Ahlberg et al., 2023). N_{INP} measured for these two categories, as well as for an intermediate category ($100 < M_{BC} < 300$ ng m^{-3}; $n = 304$), are shown in Figure 4 (panels d, e, f). The ranking of the plots is similar to what is observed when distinguishing based on the time spent in the PBL, but when using the BC as an indicator these differences are amplified. N_{INP} for "continental polluted" category is 6.5 times higher than for "continental clean". We note that polluted air masses contain twice as many particles as clean air masses (1,812 vs. 857 cm^{-3}), which can certainly have an influence on N_{INP}. From these observations, it is possible to conclude that polluted continental environments may contain substantial amounts of INPs in contrast with clean ones. Although the origin of these particles is not determined in this study, we can hypothesize about their sources. Polluted air masses are associated with longer residence times in the boundary layer, suggesting that potential INP sources could include soil dust, as reported by numerous studies for continental air masses (O'Sullivan et al., 2014; Steinke et al., 2016; Tobo et al., 2014). Another possible source is particles from biomass burning, which have been shown in several studies to possess ice-nucleating properties (Barry et al., 2021; McCluskey et al., 2014). During winter, residential wood combustion is a common heating method in Europe (Cuesta-Mosquera et al., 2024). Back trajectory analyses indicate that these air masses, characterized by high BC content, originate from eastern France and Germany, passing over many residential regions along the way. These observations underline the importance of anthropogenic as well as natural sources in influencing the INP concentration of continental air masses.

3.3. Focus on South Sector (S-Sec)

This section presents the analysis for S-sec (n = 1,586) excluding measurements done during DuEv#1 and DuEv#2. In this sector, the N_{INP} exhibit a clear correlation ($R^2 = 0.86$, $p < 0.001$ at −31°C) with M_{DUST} derived from the CAMS model (Figures 5a and 5b). These air masses, coming from arid southern regions; consistently carry elevated dust concentrations, even in the absence of strong dust events. Additionally, Figure 5b shows a very

similar temporal evolution between M_{BC} content and M_{DUST}. Even though less absorbing than BC, desert dust particles can absorb light (Bergström et al., 2007; Lafon et al., 2006). Hence, the measurement of BC content with a filter-based instrument is still a matter of debate as several studies showed a potential bias due to physical properties of measured particles (Fialho et al., 2005; Müller et al., 2011; Tinorua et al., 2024). Even if the MAAP is considered as a good instrument to reduce these artifacts (Coen et al., 2010; Petzold et al., 2005), our results tend to show that they still exist in the case of extreme dust event.

Since N_{INP} for this sector is mainly driven by dust concentration, and considering that dust is transported indiscriminately in both the boundary layer and the free troposphere, we consider for this sector all measurements whatever the BLH value at the station. On average, N_{INP} measured in S-sec are twice as high as those measured across all sectors. The average N_{AP} measured is 1,861 cm^{-3} ($\pm\sigma$ = 2,360 cm^{-3}) while the average BC content is 162 ng m^{-3} ($\pm\sigma$ = 121 ng m^{-3}). Figures 5d and 5e show the INP concentration when M_{DUST} is lower than 0.5 µg m^{-3} (n = 811) and higher than 5 µg m^{-3} (n = 195), respectively. The average N_{AP} measured are 2,494 cm^{-3} ($\pm\sigma$ = 2,908 cm^{-3}) and 799 cm^{-3} ($\pm\sigma$ = 258 cm^{-3}). BC content is 114 ng m^{-3} ($\pm\sigma$ = 87 ng m^{-3}) and 317 ng m^{-3} ($\pm\sigma$ = 60 ng m^{-3}). The choice of thresholds was based on the analysis of the M_{DUST} distribution for the southern air masses. Dust-free conditions with concentrations <0.5 µg m^{-3} represent the majority of the time, accounting for 53% of occurrences. Air masses with concentrations >5 µg m^{-3} (13% of occurrences) represent specific moments during which the dust concentration increases significantly. INP concentrations measured for high dust concentrations are, on average, more than 8 times higher than those measured for low concentrations.

4. Focus on Dust Events

Two episodes of Saharan dust were recorded during the sampling period. The first one, of moderate intensity, occurred on 16 February 2023. The second one, of greater magnitude, took place on 22–23 February. The description of the meteorological situation as well as the identification of the air mass origin through the study of back-trajectories for these two events are detailed in Appendix B. Figures 6 and 7 represent, for each event, the concentrations of INPs (N_{INP}) and dust (M_{DUST}) as well as the LIDAR measurements taken at the same time at CZ site. The LIDAR depolarization ratio is calculated at the wavelength 355 nm, in order to estimate aerosol particle concentrations (N_{AP}).

4.1. First Dust Event (DuEv#1)

Figure 6 shows a good agreement between the temporal evolution of measured INP concentrations (Figure 6a) and the LIDAR depolarization ratio (Figure 6c). Both signals increase in the afternoon of 15 February, followed by a much more pronounced second increase during 16 February. The shape of the dust plume illustrated by the modeled dust concentration vertical profile (Figure 6b) is also in accordance with LIDAR measurements (Figure 6c). The maximum depolarization ratio is reached on 16 February at 23:20 UTC, while the maximum INP concentrations are measured between 00:00 and 02:00 UTC on 17 February (645 INP L^{-1} at −33°C). However, on 17 February, N_{INP} remains at a significant level (361 INP L^{-1} at −33°C) while the depolarization ratio has decreased. We also notice that the decrease in the depolarization ratio occurs simultaneously with the appearance of a cloud below 3,000 m around midnight on 17 February (Figure 6c). This cloud subsequently led to the LIDAR shutting down multiple times. It should be noted that CZ station is located 11 km east of PUY, and during these episodes, the air masses come from the West, which may introduce a slight temporal offset between observations at these two stations. This is illustrated by Figure 6d, which represents M_{DUST} predicted by CAMS model at 1,465 m a.s.l vertically above each station. The lag corresponding to the advection time of the air mass between PUY and CZ is approximately 2 hr.

4.2. Second Dust Event (DuEv#2)

The presence of low clouds for a significant portion of the second event prevented LIDAR measurements ($RH_w \geq 100\%$ and average LWC = 0.26 g m^{-3}, at PUY on 21 and 22 February). Nevertheless, at the beginning of the episode, once again, we observe that the INP measurements (Figure 7a) and LIDAR depolarization ratio follow the same temporal evolution (Figure 7c). They increase simultaneously on 21 February around 23:00 UTC. CAMS M_{DUST} prediction (Figure 7b) shows that the increase occurs later, but the concentration peak (28 µg m^{-3}) reached between 9:00 and 11:00 UTC is relatively well correlated with INP measurement (1,023 INP L^{-1} at −33°C).

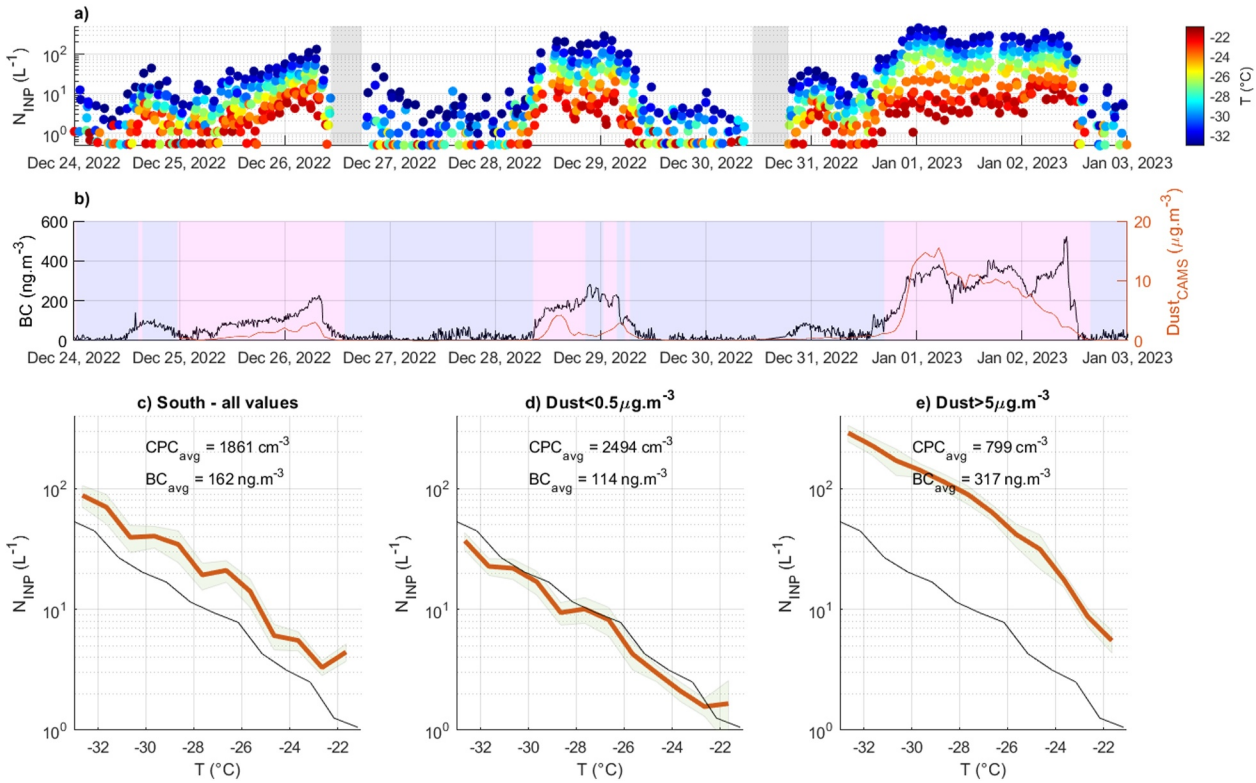

Figure 5. (a) Time series of INP concentrations measured as function of temperature at PUY between 24 December 2022 and 3 January 2023. The gray shaded areas correspond to the period of background measurements, (b) Time series of BC measurement (in blue) and CAMS dust prediction (in orange) over the same period. Red shaded and blue shaded areas represent, respectively, southerly and westerly air masses. (c) The bottom panel depicts INP averaged concentration (thick orange lines) for the southern sector, (d) for the predicted dust concentration below 0.5 μg m^{-3}, and (e) for predicted dust concentration higher than 5 μg m^{-3}. The thin black line represent the average value over the entire campaign (as in Figure 2). The shaded areas on panels (c)–(e) represent the 95% confidence interval.

During the second part of the event, even though the M_{DUST} remains at a significant level (>5 μg m^{-3}), it has decreased noticeably down to ≈10 μg m^{-3}, while the INP concentrations remain at a very high level on 23 February (1,028 INP L^{-1} at −33°C). We note that the LIDAR operated for 50 min on 23 February from 12:00 UTC, and that, at this moment, the depolarization ratio is high (0.026), in agreement with INP measurements. Then, we observe a last peak in INP measurements at the end of the event on the morning of 24 February, which cannot be correlated with dust concentration. We remind here that the dust concentration is derived from the CAMS model and is not measured at the station. The comparison with LIDAR shows that there can be a time offset of several hours. Thus, discrepancies between dust concentration and measured INP concentrations may come from the uncertainty of the model and its limited spatiotemporal resolution. For this event, according to M_{DUST} prediction as depicted in Figure 7d, the advection time of the air mass between PUY and CZ is approximately 1 hr.

During these two dust events, the average INP concentration measured at −33°C were 477 L^{-1} ($\pm\sigma$ = 350 L^{-1}, n = 30) reaching an absolute maximum value of 1,229 L^{-1}. We can compare these values with those measured close to the source emissions during dust event in 2013 at the Izaña station (2,373 m a.s.l, Canary Islands) (Boose et al., 2016). The maximum average night concentration reported during dust events was 367 L^{-1} (at −33°C and RH_w ≈ 105%) with a dust concentration of 15 μg m^{-3}. They also reported an absolute maximum INP values greater than 2,500 L^{-1}. Despite being based on a single comparison of measurements done at different time periods and potentially under different meteorological conditions, this might suggest that the INP properties of a dust plume, during extreme events, do not depend on the transport duration, this was previous demonstrated by Denjean et al. (2016), for other aerosol properties (concentration and size distribution) of African mineral dust after intercontinental transport.

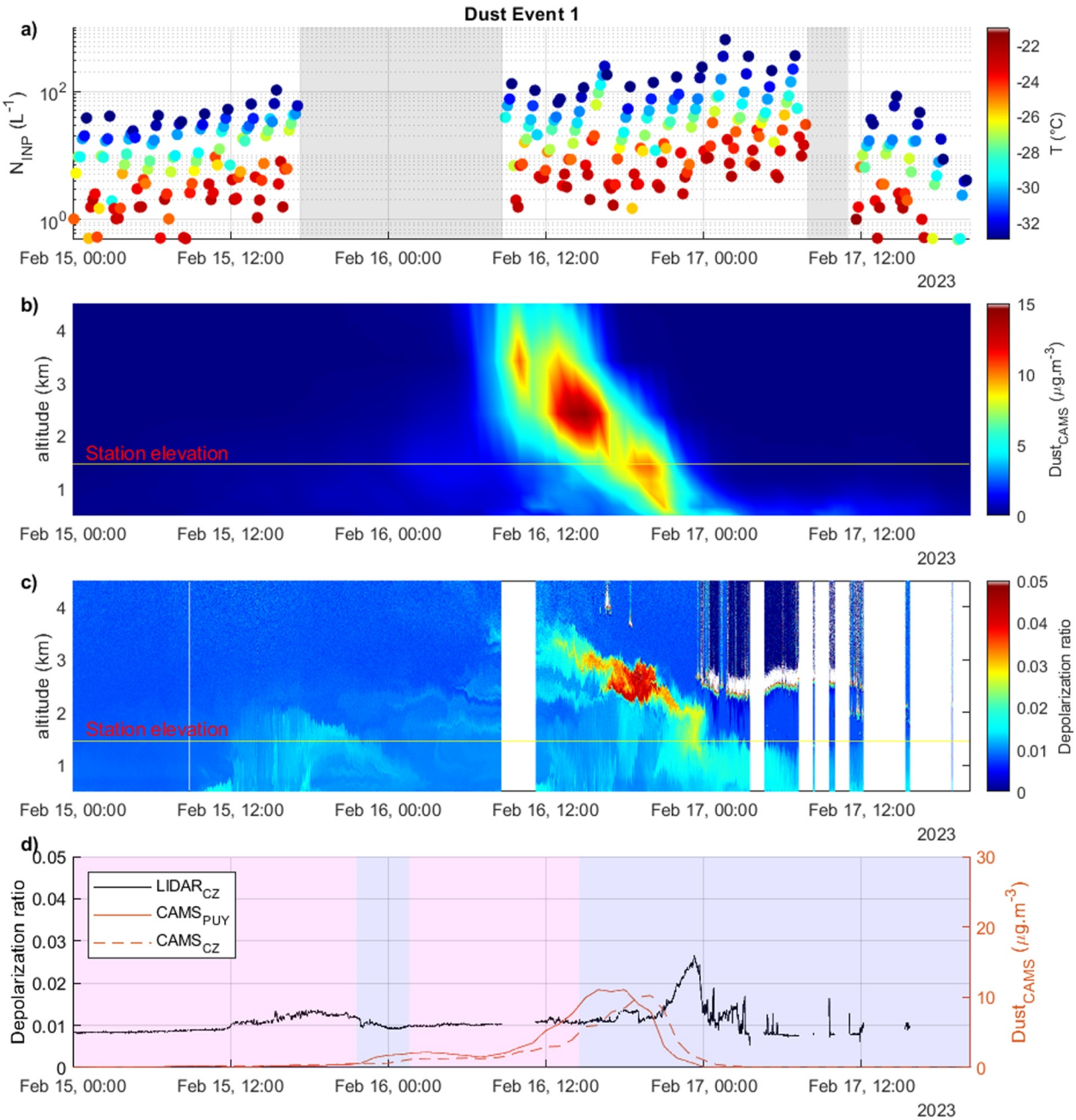

Figure 6. Temporal evolution of parameters characterizing the first dust event (DuEv#1) which occurred from 16 to 17 February 2023. (a) INP concentration measured at PUY, (b) vertical profile of dust concentration predicted by CAMS model at the location of CZ, (c) vertical profile of LIDAR depolarization ratio at 355 nm at CZ. The white areas correspond to periods when the LIDAR is not measuring due to the presence of low level clouds. When the backscattered intensity is too high, the system shuts down as a protective measure, and (d) LIDAR depolarization ratio at the altitude of PUY (in black), CAMS dust concentration prediction (at CZ and PUY, in orange). The colored shaded areas indicate the air mass origin as in Figure 5.

5. Development of New Parameterizations for Heterogeneous Ice Nucleation

In this work, we developed several parameterization sets (depending on one or two parameters) to characterize heterogeneous ice nucleation for different air masses. For this purpose, we selected four specific types of air masses (oceanic, continental polluted, continental free troposphere, southern heavily loaded with dust particles concentration >5 μg m^{-3}), described in Sections 3, and representing the N_{INP} variability observed during the

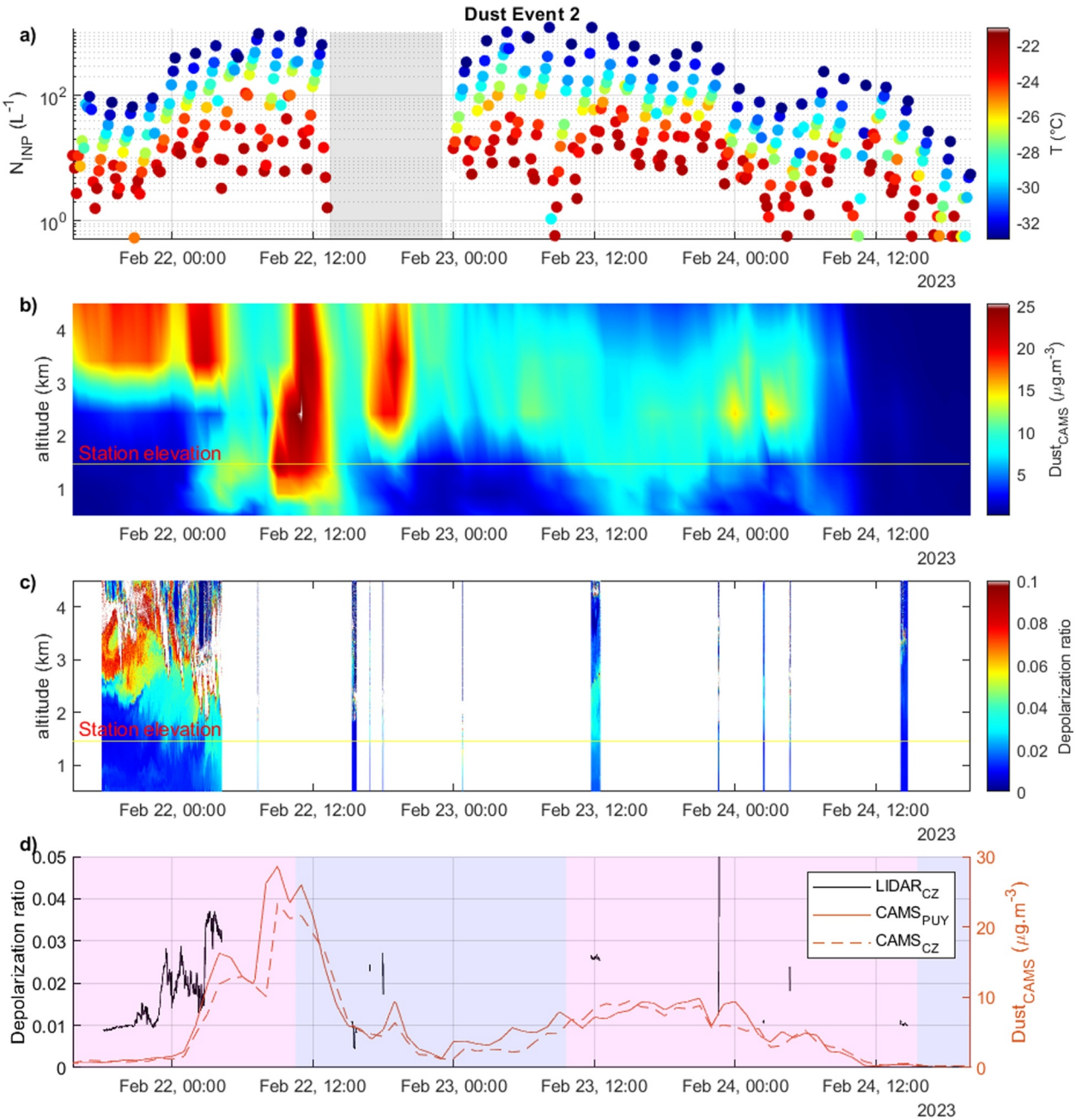

Figure 7. Same as Figure 6 for DuEv#2.

campaign. We also developed a parameterization "Dust event" based on the peak values observed during the second dust event (DuEv#2) on 22 February.

For single-parameter parameterizations, we used an exponential expression as a function of air temperature T_k (in K) (Equation 1) or as a function of the saturation with respect to the ice phase S_i (Equation 2) as proposed by Meyers et al. (1992), for which we redefined a new set of coefficients for each type of air mass.

$$N_{\mathrm{INP}} = \exp\left[a_{(1)} + b_{(1)}\left(273.15 - T_k\right)\right] \quad (1)$$

$$N_{\mathrm{INP}} = \exp\left\{a_{(2)} + b_{(2)}\left[100\left(S_i - 1\right)\right]\right\} \quad (2)$$

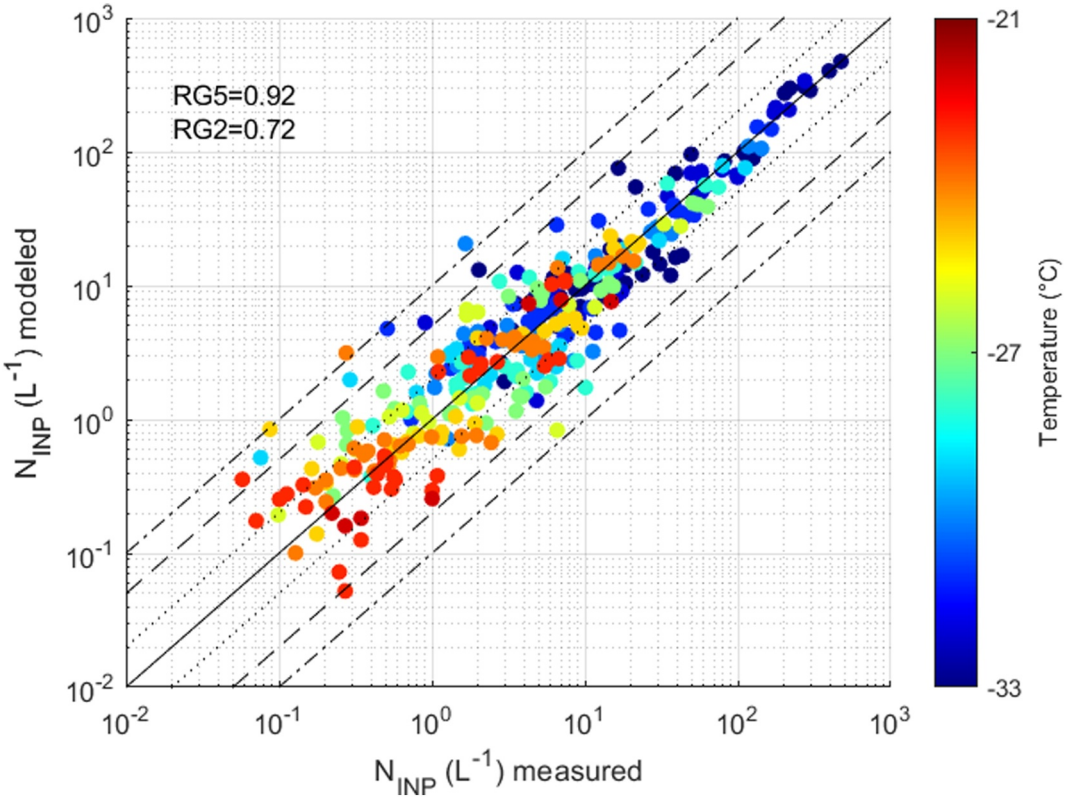

Figure 8. Predicted INP concentrations using the combination of newly developed parameterizations (Equation 3) versus measured INP concentrations for the entire campaign. The solid line, dotted lines, dashed lines and dash-dotted lines represent respectively the 1:1 ratio line, the 1:2 ratio lines, the 1:5 ratio lines, and the 1:10 ratio lines.

These exponential laws fit well with the observations (Figure C1, $R^2 > 0.96$). The considered temperature T_k is the temperature at which the measurement is conducted. The value of S_i is obtained by considering water saturation at the measurement temperature, which is consistent with the machine's operating mode. It can be observed that they accurately reproduce the average concentrations of INPs for different air masses as well as their relative positioning. However, a parameterization based on a single parameter does not reproduce all the variability of the measured concentrations with temperature for a given air mass.

We also use a two-parameter parameterization proposed by Bras et al. (2024) (called hereafter B24; Equation 3) based on offline measurements conducted at the same site (PUY) during the WINS campaign (November 2018 to May 2019).

$$N_{INP} = [a * \ln(N_{AP}) + b] * \exp[c\,(273.15 - T_k) + d] \quad (3)$$

This equation expressing N_{INP} (L^{-1}) considers, in addition to temperature (T_k in K), the total concentration of aerosol particles (N_{AP} in cm^{-3}) rather than the concentration of aerosols with a diameter larger than 500 nm ($N_{aer,500}$) as in the DeMott et al. (2010) (called hereafter D10) and DeMott et al. (2015) (called hereafter D15) parameterizations. This choice is constrained for two reasons: (a) size distribution of aerosol particles was not available, and (b) total aerosol number concentration is a required variable at all ACTRIS national facilities, making it widely available for integration into future parameterizations. Figure 8 depicts the predicted data from our new set of parameterizations versus the associated measured data for the entire campaign. It shows that 72% of INP concentrations are predicted by the parameterization set within a factor of two of the observed data (RG2), and 92% of points are predicted within a factor of 5 (RG5). The highest discrepancies between modeled and measured concentrations occur for temperatures above −25°C and concentrations lower than 1 INP L^{-1}. This can be explained by the limit of detection of the PINE, which is 0.5 L^{-1}. There are also a few points for which the

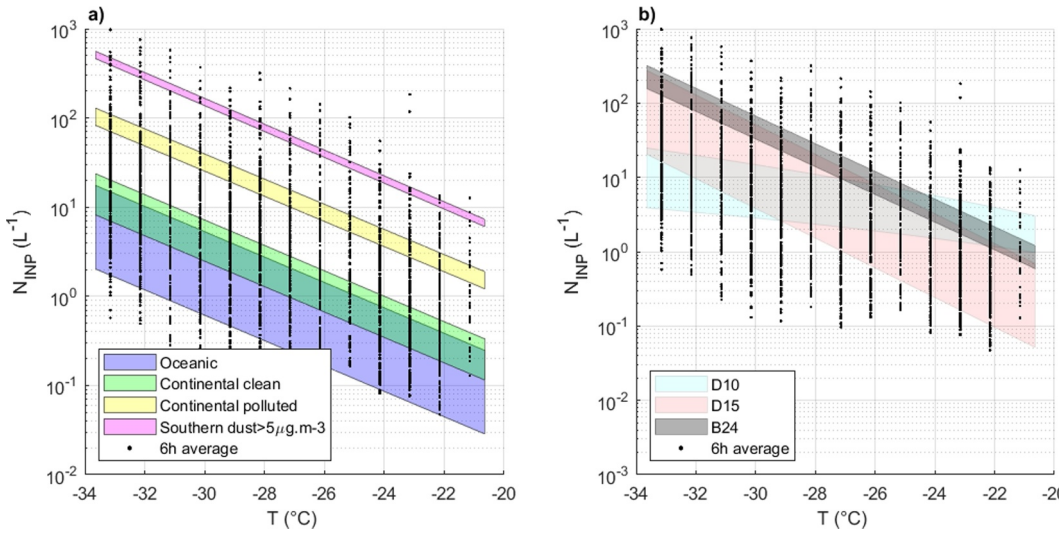

Figure 9. (a) INP predicted values of the newly developed parameterizations (based on Equation 3) as a function of the temperature. For each air mass type, we considered the first and the last percentile of the total particle concentration for each air mass type as the min and max values for N_{AP}, and (b) same as in panel (a) but for existing parameterizations.

measured value is null. These points cannot be shown on Figure 8 due to the logarithmic scales, but they are taken into account when performing the fits.

Figure 9a represents the values provided by all parameterizations as a function of temperature, along with the daily averages measured for the entire campaign. We can see that the use of several parameterizations makes it possible to represent the high variability of measured concentrations in varying conditions. We observe that the parameterizations do not represent all the values measured during the campaign. Since the focus is on certain specific air masses, only these are represented. Indeed, a significant number of measurement points were excluded to conduct this analysis. The values obtained with the oceanic parameterization cover one order of magnitude for a given temperature which is significantly more than for the other parameterizations. This is a result of a wider range of total particle concentration measured for that class of air mass. The fitted values of the coefficients for the new parameterizations are synthetized in Table 2. More details about parameterizations are given in Appendix C.

Here, the proposed parameterizations are compared with existing parameterizations (B24, D10, and D15). The values provided by the different parameterizations between −23°C and −33°C are shown in Figure 9b. For B24, we considered the Oceanic average particle concentration as the lowest value and the average "Continental polluted" particle concentration as the highest. For D10 and D15, as PSD were not available for this study, we used the range of $N_{aer,500}$ [0.5, 4 cm^{-3}] reported by Bras et al. (2024) based on measurement conducted at PUY during the same period of the year. It is important to remember here that the B24 parametrization was developed based on offline measurements collected over a 6 month period for temperatures between −5°C and −18°C. Therefore, it is used here outside its characterization range. We observe that the values provided by this parameterization are relatively high and close to air masses of the "continental polluted" type. The same behavior is observed for the amplitude related to variations in aerosol particle concentrations. The D10 parameterization shows a very different behavior with temperature. Below −30°C, it provides relatively low values, close to the "oceanic" case. In contrast, beyond −24°C, the values are relatively high and exceed those for the "continental polluted" case. The D15 parameterization provides intermediate values covering a large part of the measured values during campaign and seems to be more accurate in this case than the D10. However, since the aerosol size distribution was not measured during the campaign, making more precise comparisons with these last two parameterizations is not possible, as they can be influenced by the assumptions made for the $N_{aer,500}$ estimation. This point will be addressed in future work, using both an SMPS and super micron particles size measurements in parallel with INP measurements.

To evaluate this new set of parameterizations, we used five different datasets. These include the two datasets presented by Wilbourn et al. (2024), based on PINE measurements at SGP and ENA, and a dataset from the

Table 2
Fitted Values of Coefficients for Each Type of Air Mass and for the Parameterizations Expressed With Equations 1–3

Air mass class	$a_{(1)}$	$b_{(1)}$	$a_{(2)}$	$b_{(2)}$	$a_{(3)}$	$b_{(3)}$	$c_{(3)}$	$d_{(3)}$
Oceanic	−9.6462	0.3459	−8.7882	0.2830	1.1805e−4	−4.5172e−4	0.3277	−0.5885
Continental clean	−8.9846	0.3577	−8.0946	0.2925	3.1487e−7	−8.8237e−7	0.3281	5.4433
Continental polluted	−6.0507	0.3187	−5.2584	0.2606	9.8069e−3	−4.5234e−2	0.3247	−2.6872
Southern $dust_{conc} > 5$ μg m^{-3}	−4.7525	0.3257	−3.9304	0.2659	0.31401	5.6970e−2	0.3337	−5.8141
Dust event	−4.7290	0.3538	−3.8369	0.2890	–	–	–	–

HyICE (Hyytiälä Aerosol-cloud Experiment) campaign (Vogel et al., 2024), which reported PINE measurements in a Finnish boreal forest. Additionally, we used a dataset from the PICNIC campaign at PUY, based on PINE measurements (Lacher et al., 2024). Lastly, we incorporated the measurements presented by DeMott et al. (2016, hereafter D16), obtained from various field campaigns in marine environments using diverse measurement methods. For the PICNIC dataset at PUY, we applied the same method presented in this work, based on air mass classification. Since no dust or oceanic events occurred during this campaign, we applied the continental parameterizations to this dataset. Similarly, we used the continental parameterizations for the SGP and HyICE campaigns, as these sites are reported to be continental. Finally, we applied the oceanic parameterization to compare with the ENA and D16 measurements. The results, depicted in Figure 10, indicate that the parameterizations predict, on average, 61% of N_{inp} of the combined dataset within a factor 5%, and 79% within a factor 10. We note that the results for the PICNIC campaign, conducted at the same site but during a different period, are good, with 100% of NINP predicted within a factor of 5. This is partly due to the application of the exact same method for data processing based on air mass analysis. It is also worth mentioning that the oceanic parameterization overestimates the D16 measurements while underestimating ENA's, particularly at temperatures warmer than −18°C, which fall outside the temperature range measured in this study.

6. Conclusions

The measurements of INP concentrations were conducted continuously (time resolution ≈ 10 min) during the winter of 2023 at the summit of Puy de Dôme (PUY site) over a period of 3 months, resulting in 11,869 data points. These measurements were carried out using a PINE type cloud chamber, over a temperature range between −22°C and −33°C. These measurements are analyzed with systematic 72 hr back-trajectories of sampled air masses over the entire period. This approach holds significant value, as it makes possible the comparison of INP

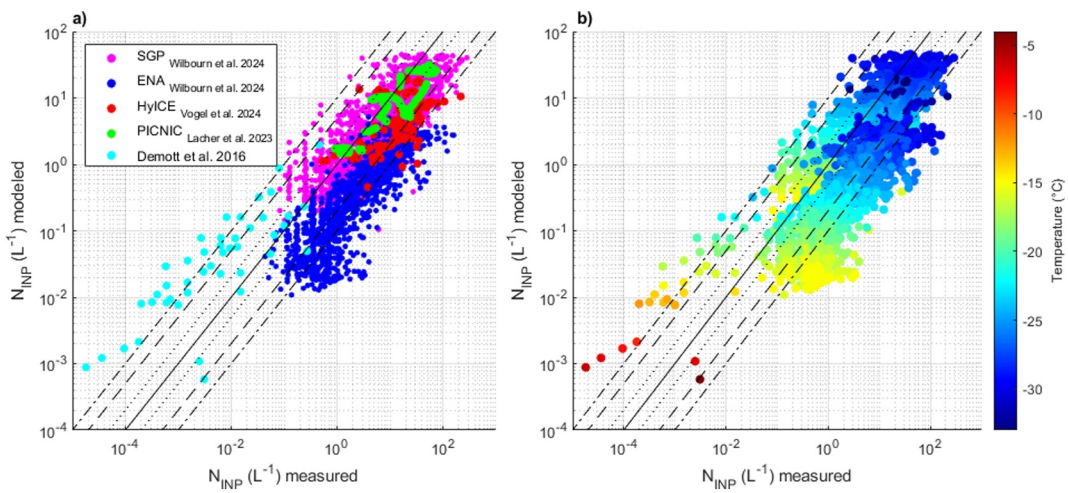

Figure 10. (a) Predicted INP concentrations using the combination of newly developed parameterizations (Equation 3) versus measured INP concentrations from various field campaigns reported in the literature, and (b) same as in panel (a), the colors represents the measurement temperature.

concentrations of various air mass types at a single site. Therefore the comparison can be made without any bias introduced by the use of differing analytical approaches (Lacher et al., 2024).

INP concentrations characterization is done for four specific air mass classes: representative of "oceanic," "continental clean," "continental polluted," and "southern loaded with dust." Desert dust is known to be efficient INPs, especially at low temperatures that were studied in this work on a global scale. This study confirms that the contribution of dust to ice nucleation activity following long-range transport is significant based on our back trajectory analysis, and that the proposed method effectively identifies these sources. Oceans also represent a significant source of INPs in the atmosphere, although they tend to be less INP active than other sources, consistent to previous findings (e.g., Vergara-Temprado et al., 2018). Consequently, in regions where other sources predominate (over the European continent), these marine sources become insignificant contributors to INP concentrations. However, in regions with few aerosol sources, such as over the open oceans, these oceanic sources of INPs dominate. Even though PUY is not located in a coastal region, a large fraction of air masses in winter are coming from west after traveling over Atlantic ocean, inducing a marine signature in ambient INP concentrations by applying selective criteria to air mass analysis (residence time in the MBL, reduced transport time from the ocean, and limited residence time in the PBL). Given the location of PUY, we also have the opportunity to assess the importance of marine INP sources compared to dust or continental sources.

We applied the same method for continental air masses and segregated them based on their pollution level. A strong correlation between INP concentration and BC content was observed. It has been previously shown that BC measurements can be biased by the presence of dust. However, for continental air masses, dust concentrations are very low (<0.6 μg m^{-3}) and therefore not correlated with BC ($R^2 \approx 0$). It illustrates that polluted continental air masses, with longer residence times in the BL, are associated with a higher total number of particles and larger INP concentrations, confirming the contribution of anthropogenic emission to the INP population.

The main drawback of our methodology is that it requires a large number of measurements to obtain samples of significant size after applying the selection criteria. This is especially true for measurements of air masses with low INP concentrations (i.e., "oceanic" and "continental clean" cases) in the upper temperature range (>-25°C) because of the detection limit of the PINE. However, as PINE operates is an autonomous and continuous fashion enabling long-term measurements, making the collection of a large number of data points is possible.

Another drawback is that size distribution of aerosol particles were not available during the campaign. This prevents us from properly evaluating parameterizations based on aerosol size or total surface area and thus, from developing parameterizations using the same approach.

In this work, we propose several parameterizations representing heterogeneous ice nucleation for each type of air masses. These parameterizations use equations proposed by Meyers et al. (1992) and Bras et al. (2024). Results show that the new set of parameterizations makes possible to represent the large variability of INP concentrations as a function of air mass type. The use of two parameters (temperature and particle total concentration) instead of only one (temperature or ice saturation ratio) improves the representation of each parameterization.

Nevertheless, we show that the variability is largely explained by the segregation of air mass type (Burrows et al., 2022), which incorporates many other parameters (chemical composition, size distribution, coating, aging) and not only the total particle concentration. INP measurements are still continuously conducted at PUY. Furthermore, other aerosol measurements such as size distribution, chemical, and biological composition analysis, are planned to be conducted in parallel. This will enable the use of a size parameter in the development of future parameterizations. The analysis of chemical composition will also improve understanding of the drivers of INP concentration and help refine criteria for air mass classification to obtain more specific and/or new classes.

Future work will include implementing these parameterizations into mesoscale models using either bulk or bin microphysics representation (WRF, Méso-NH or DESCAM). This will enable the assessment of the role of heterogeneous ice nucleation, as a function of the INP emissions source, on cloud properties across various environments.

Appendix A

Figure A1 shows the time series of the measured INP concentration, the total particle number, and BC mass content. It also indicates the origin of air masses according to the three sectors (W-sec, S-sec, and NE-sec), as well as the different episodes for the specific air mass classes analyzed in Section 3.

Figure A2 shows the number or runs performed for each temperature bin ($\Delta Tc = 1°$) as well as the number of runs for which zero values are measured. The ratio of zero values highly depends on N_{INP} and then on temperature,

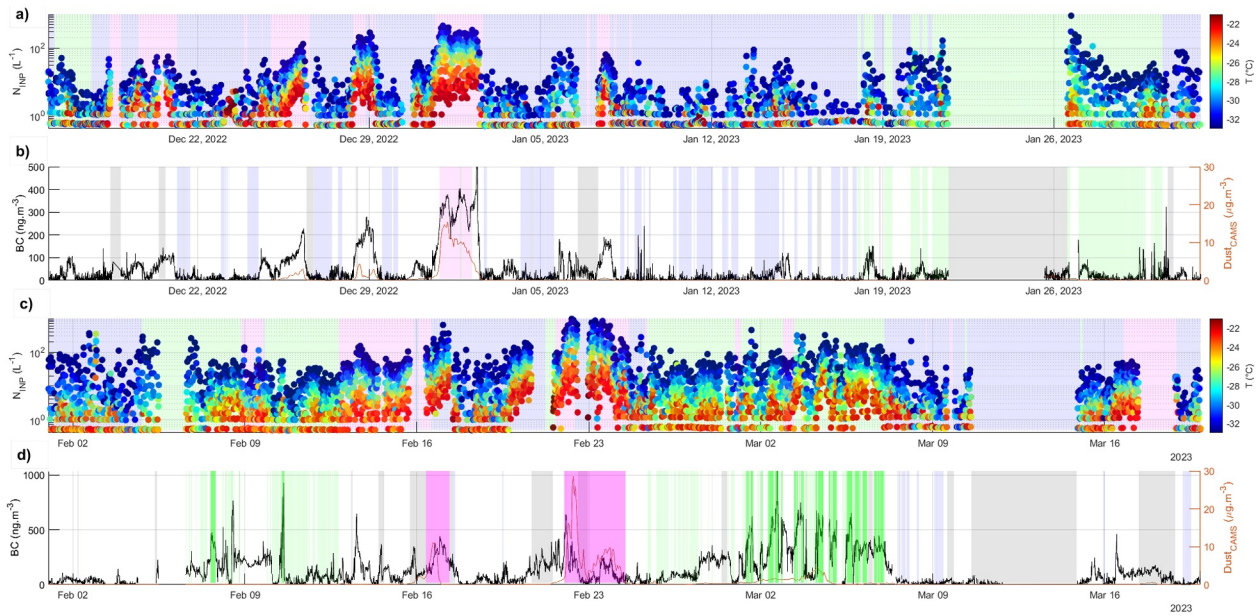

Figure A1. Time series over the entire campaign for INP concentrations (panels (a) and (c)). The red, blue, and green shaded areas represent, respectively, southerly, westerly, and northerly air masses. Panels (c) and (d) represent black carbon mass content and dust concentration. The red, blue, light green, dark green, and magenta shaded areas represent, respectively, southern (dust >5 μg m^{-3}), oceanic, continental clean, continental polluted, and dust episodes. The gray shaded areas indicate background procedures and the two periods when PINE was not operational.

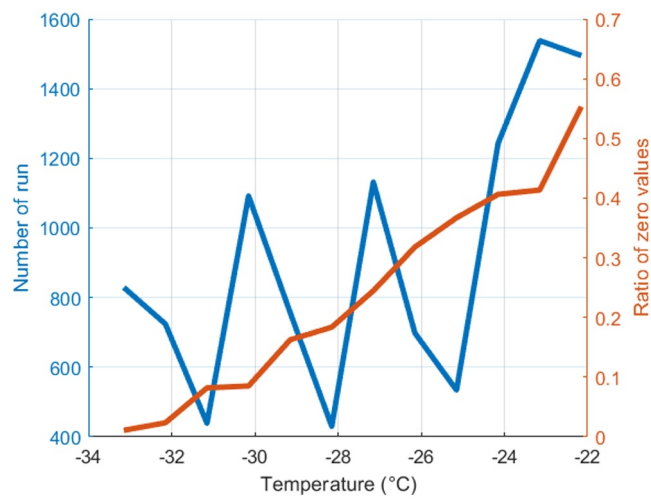

Figure A2. In blue, number of measurement taken for each temperature bin. In orange, ratio of runs for which zero INP are detected as a function of temperature.

Table A1
List of Instrumentation and Models Used

Instrument	Model (manufacturer)	Acquisition time	Detection limit	Max concentration	Size range	Uncertainty
Particle counter	CPC 3010 (TSI)	1 Hz	0	10,000 cm^{-3}	>10 nm	±10%*
Particle absorption	MAAP 5012 (Thermo)	10 min	50 $ng.m^{-3}$	180 $\mu g.m^{-3}$	$PM_{2.5}$	10%*
INP counter	PINE-05-01 (Bilfinger Noell GmbH)	10 min	0.5 L^{-1}		4 µm	20%
Dust concentration	Copernicus Atmosphere Monitoring Service (CAMS)—ENSEMBLE	1 hr	NA	NA	PM_{10}	Spatial resolution (0.1°)

*Instrument calibrated and certified by CEN standards at the ECAC calibration center (https://www.actris-ecac.eu/measurement-guidelines.html, last access 02/07/2024).

exceeding 0.5 at −22°C when the average N_{INP} measured is lower than the instrument's limit of detection (0.5 L^{-1}).

Table A1 lists the characteristics (model, manufacturer, acquisition time, detection limit, size range, uncertainty) of the instruments and models used in this study. In this study, we use the total particle concentrations averaged over a duration of 5 min.

Appendix B

According to the CAMS forecast, the Calima wind transported Saharan dust to the Canary Islands on 13 February. The dust transport continued northward on 14–15 February. Then the dust plume reached Ireland and the UK. The analysis of back-trajectories on these dates (Figure B1a) shows air masses originating from North Africa and having crossed over Spain at the beginning of the event. The origin of the air mass then gradually shifts westward with a passage over the Canary Islands and then over the Atlantic Ocean at the end of the event.

The second event is actually just a continuation of the first one, with the Calima wind continuing to blow in the following days generating a dust transport reaching Denmark. The back-trajectories from the CAT model (Figure B1b) also show an origin from North Africa with a passage over Spain and the Pyrenees, which is consistent with the concentrations recorded at that period in these areas.

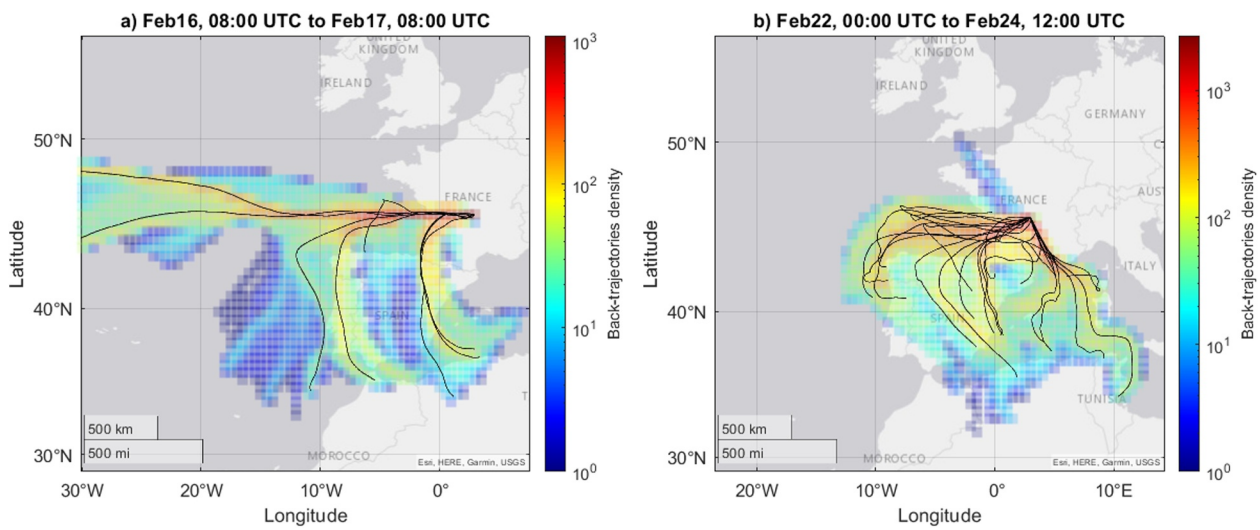

Figure B1. The colors represent the 72 hr back-trajectories density during dust events #1 (DuEv#1) (a) and #2 (DuEv#2) (see Section 4), and (b) averaged on a 0.5° grid in lat-long. The black lines illustrate samples of back-trajectories during the event (1 every 3 hr).

Appendix C

To obtain the parameterizations following equations (Equation 1) and (Equation 2) proposed by Meyers et al. (1992), we fitted the experimental data for each air mass type, averaged over 1°C bins, as presented in

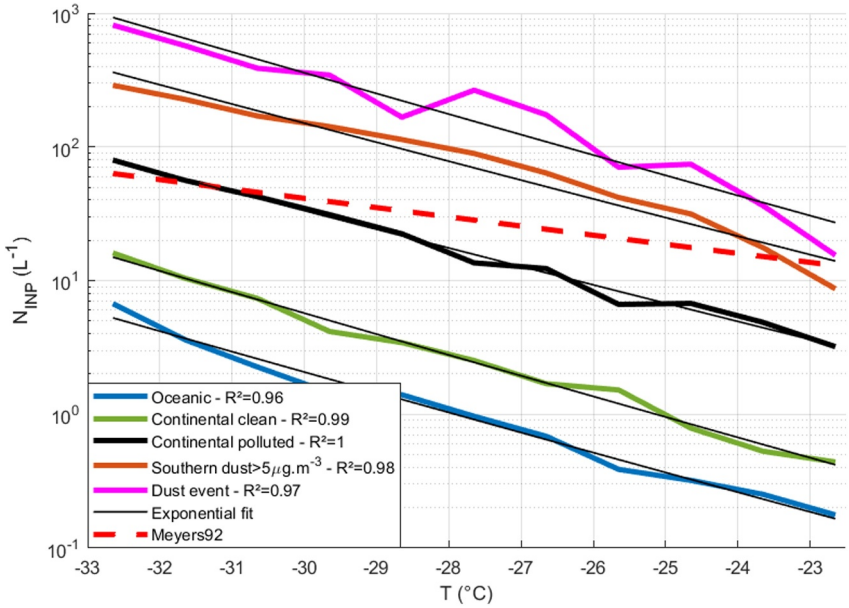

Figure C1. INP measured concentrations (colored thick lines) for each air mass class as a function of temperature represented with associated exponential parameterization (black thin lines) following equations (Equation 1) and (Equation 2).

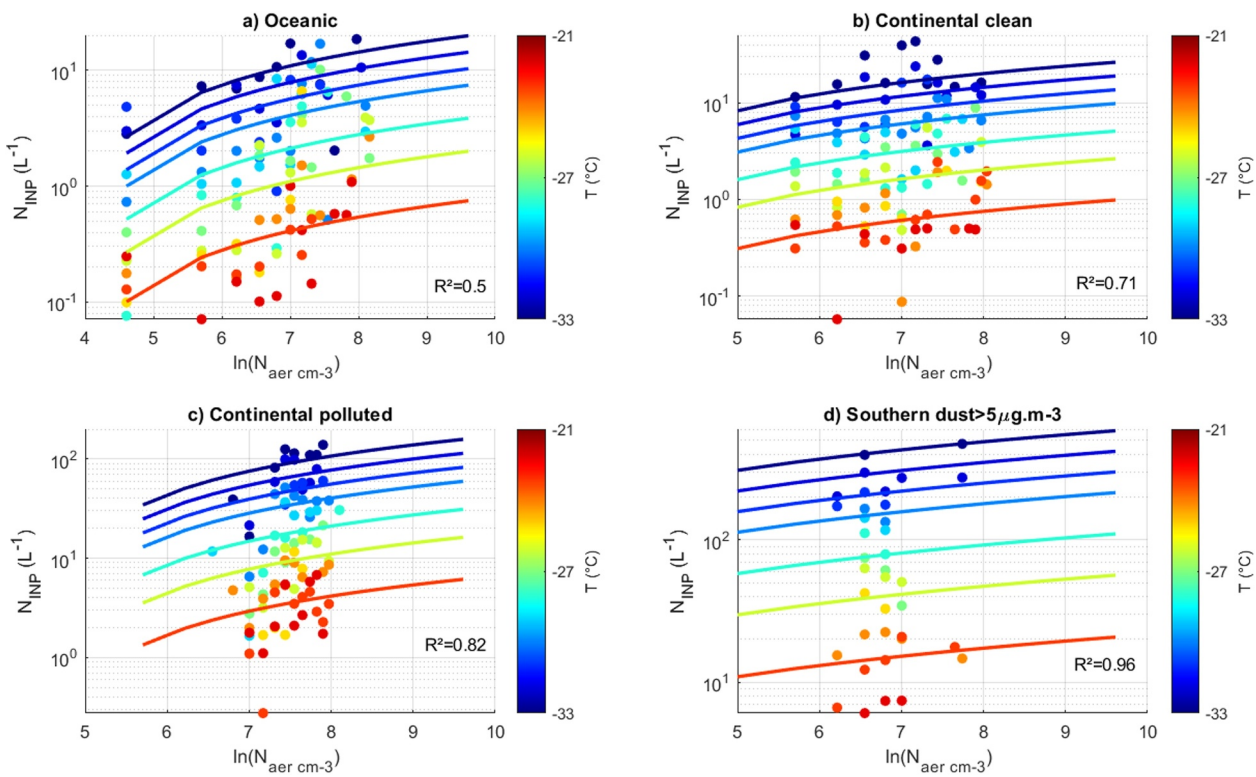

Figure C2. INP measured concentration for each air mass class as a function of N_{AP} and temperature (circles) represented with associated parameterization (lines) following Equation 3. (a) "Oceanic", (b) "Continental Clean", (c) "Continental polluted", and (d) "Southern dust" >5 μg m^{-3}.

Section 3. We used a classic nonlinear least squares algorithm for this purpose. The results are presented in Figure C1, showing a good correlation between measurements and fitted parameterizations, with correlation coefficients (R^2) greater than 0.96 in every case. However, we can see that the model struggles to reproduce the shape of the measurements for the dust cases at temperatures warmer than −23°C. INP concentrations calculated using the parameterization from Meyers et al. (1992) are also displayed in the figure.

As the expression of S_i as a function of temperature T is bijective and both equations have an exponential form, their fit to the experimental results gives the same values. Only the coefficients differ. The S_i value is derived from temperature considering the RH_w is equal to 100%. As the RH_{max} value during the expansion is assumed to be $100\% < RH_{max} < 102\%$ and that the incertitude in the measured temperature is ±1°C. This lead to an incertitude on $RH_i < 3\%$ on the temperature range (from −22°C to −33°C). S_i is obtained by the ratio $e_{sat,w}/e_{sat,i}$, where $e_{sat,w}$ and $e_{sat,i}$ are the saturation partial pressures of water vapor with respect to water and ice, respectively, given by Tetens formula (Tetens, 1930): $e_{sat}(T) = \alpha_1 * \exp\{\alpha_3 (T - T_0)/(T - \alpha_4)\}$ with the parameters set according to Buck (1981) for saturation over water ($\alpha_1 = 611.21$ Pa, $\alpha_3 = 17.502$ and $\alpha_4 = 32.19$ K) and to the AERKi formula of Alduchov and Eskridge (1996) for saturation over ice ($\alpha_1 = 611.21$ Pa, $\alpha_3 = 22.587$ and $\alpha_4 = -0.7$ K), with $T_0 = 273.16$ K (see 17,117-part-iv-physical-processes.pdf (ecmwf.int)).

For the dust event parameterization, we used the average values over a 6 hr period during the peak of the second event DuEv#2 (22 February, from 6:00 to 12:00 UTC).

To obtain the parameterizations following Equation 3 proposed by Bras et al. (2024), we fitted the experimental data for each air mass type, averaged over 1°C bins for temperature and 200 cm^{-3} bins for total particle concentration, and weighted by the number of observations. We also implemented the previously used nonlinear least squares algorithm.

The results are presented in Figure C2, having correlation coefficient R^2 over 0.7 except for the oceanic case (0.5). Indeed, for this air mass class, as it can be seen in Figure C2, the representation of the temperature effect is not completely monotonic. This suggests, like already mentioned in Section 3.1, that this class is still slightly perturbed by other parameters linked to anthropogenic/dust emissions. Hence, applying some more restrictive criteria (i.e., BC and dust concentration) to the air mass classification could lead to a better representation and a better focus on purely marine environments.

We can also notice that the range covered by the N_{AP} parameter is not the same in all classes. It is notably quite limited for the 'southern dust' >5 µg m^{-3} class. Given that Equation 3 used here can yield negative values at low concentrations, it is necessary to specify a limit for N_{AP} below which the parameterization should not be used. This limit is set at 75 cm^{-3} for the "oceanic" class, 150 cm^{-3} for the "continental clean" class, and 400 cm^{-3} for the two latter classes according to measurements.

Conflict of Interest

The authors declare no conflicts of interest relevant to this study.

Data Availability Statement

Database containing INP concentration (N_{INP}), measurement temperature, total particle concentration (N_{AP}), Dust concentration (M_{DUST}), and air mass classification for the entire campaign from back trajectory analysis are provided by Canzi et al. (2024).

References

Ahlberg, E., Ausmeel, S., Nilsson, L., Spanne, M., Pauraitė, J., Nøjgaard, J. K., et al. (2023). Measurement report: Black carbon properties and concentrations in southern Sweden urban and rural air – The importance of long-range transport. *Atmospheric Chemistry and Physics*, *23*(5), 3051–3064. https://doi.org/10.5194/acp-23-3051-2023

Alduchov, O. A., & Eskridge, R. E. (1996). Improved Magnus form approximation of saturation vapor pressure. *Journal Applied Meteorology*, *35*(4), 601–609. https://doi.org/10.1175/1520-0450(1996)035<0601:imfaos>2.0.co;2

Baray, J., Bah, A., Cacault, P., Sellegri, K., Pichon, M., Deguillaume, L., et al. (2019). Cloud Occurrence Frequency at Puy de Dôme (France) Deduced from an Automatic Camera Image Analysis: Method, Validation, and Comparisons with Larger Scale Parameters. *Atmosphere*, *10*(12), 808. https://doi.org/10.3390/atmos10120808

Baray, J., Deguillaume, L., Colomb, A., Sellegri, K., Freney, E., Rose, C., et al. (2020). Cézeaux-aulnat-opme-Puy de Dôme: A multi-site for the long-term survey of the tropospheric composition and climate change. *Atmospheric Measurement Techniques*, *13*(6), 3413–3445. https://doi.org/10.5194/amt-13-3413-2020

Acknowledgments

This work was supported by the National Research Agency under the JCJC program "ANR-21-CE01-0003", and under the France 2030 program (Obs4Clim) "ANR-21-ESRE-0013." The lead author is funding by the ACME project (ANR-21-CE01-0003). The authors wish to also acknowledge CNRS-INSU for supporting measurements performed at the SI-COPDD, and those within the long-term monitoring aerosol program SNO-CLAP, both of which are components of the ACTRIS French Research Infrastructure, and whose data is hosted at the AERIS data center (https://www.aeris-data.fr/). The authors gratefully acknowledge support provided by Patrick Freville for LIDAR measurements. LIDAR measurement at CZ station are available at https://www.icare.univ-lille.fr/login/?prourl=/asd-content/archive/ (free registration). The authors wish to also acknowledge the Copernicus Atmosphere Monitoring Service (CAMS) from which dust concentration (M_{DUST}) were obtained: METEO FRANCE, Institut national de l'environnement industriel et des risques (Ineris), Aarhus University, Norwegian Meteorological Institute (MET Norway), Jülich Institut für Energie-und Klimaforschung (IEK), Institute of Environmental Protection—National Research Institute (IEP-NRI), Koninklijk Nederlands Meteorologisch Instituut (KNMI), Nederlandse Organisatie voor toegepast-natuurwetenschappelijk onderzoek (TNO), Swedish Meteorological and Hydrological Institute (SMHI), Finnish Meteorological Institute (FMI), Italian National Agency for New Technologies, Energy and Sustainable Economic Development (ENEA) and Barcelona Supercomputing Center (BSC) (2022): CAMS European air quality forecasts, ENSEMBLE data. Copernicus Atmosphere Monitoring Service (CAMS) Atmosphere Data Store (ADS) (Accessed on <13-oct-2023>), https://ads.atmosphere.copernicus.eu/cdsapp#!/dataset/cams-europe-air-quality-forecasts?tab=overview.

Barry, K. R., Hill, T. C. J., Levin, E. J. T., Twohy, C. H., Moore, K. A., Weller, Z. D., et al. (2021). Observations of ice nucleating particles in the free troposphere from western US wildfires. *Journal of Geophysical Research: Atmospheres*, *126*(3). https://doi.org/10.1029/2020jd033752

Bergström, R. W., Pilewskie, P., Russell, P. B., Redemann, J., Bond, T. C., Quinn, P. K., & Sierau, B. (2007). Spectral absorption properties of atmospheric aerosols. *Atmospheric Chemistry and Physics*, *7*(23), 5937–5943. https://doi.org/10.5194/acp-7-5937-2007

Bezděk, A., & Sebera, J. (2013). Matlab script for 3D visualizing geodata on a rotating globe. *Computers and Geosciences*, *56*, 127–130. https://doi.org/10.1016/j.cageo.2013.03.007

Bi, K., McMeeking, G. R., Ding, D. P., Levin, E. J. T., DeMott, P. J., Zhao, D. L., et al. (2019). Measurements of ice nucleating particles in Beijing, China. *Journal of Geophysical Research: Atmospheres*, *124*(14), 8065–8075. https://doi.org/10.1029/2019jd030609

Bigg, E. K. (1953). The formation of atmospheric ice crystals by the freezing of droplets. *Quarterly Journal of the Royal Meteorological Society*, *79*(342), 510–519. https://doi.org/10.1002/qj.49707934207

Boose, Y., Sierau, B., García, M. I., RodríGuez, S., Alastuey, A., Linke, C., et al. (2016). Ice nucleating particles in the saharan air layer. *Atmospheric Chemistry and Physics*, *16*(14), 9067–9087. https://doi.org/10.5194/acp-16-9067-2016

Bras, Y., Freney, E., Canzi, A., Amato, P., Bouvier, L., Pichon, J., et al. (2024). Seasonal variations, origin, and parameterization of Ice-Nucleating particles at a mountain station in central France. *Earth and Space Science*, *11*(6). https://doi.org/10.1029/2022ea002467

Brunner, C., Brem, B. T., Coen, M. C., Conen, F., Hervo, M., Henne, S., et al. (2021). The contribution of Saharan dust to the ice-nucleating particle concentrations at the High Altitude Station Jungfraujoch (3580 m a.s.l.), Switzerland. *Atmospheric Chemistry and Physics*, *21*(23), 18029–18053. https://doi.org/10.5194/acp-21-18029-2021

Brunner, C., & Kanji, Z. A. (2021). Continuous online monitoring of ice-nucleating particles: Development of the automated Horizontal Ice Nucleation Chamber (HINC-auto). *Atmospheric Measurement Techniques*, *14*(1), 269–293. https://doi.org/10.5194/amt-14-269-2021

Buck, A. L. (1981). New equations for computing vapor pressure and enhancement factor. *Journal of Applied Meteorology*, *20*(12), 1527–1532. https://doi.org/10.1175/1520-0450(1981)020<1527:nefcvp>2.0.co;2

Burrows, S. M., McCluskey, C. S., Cornwell, G. C., Steinke, I., Zhang, K., Zhao, B., et al. (2022). Ice-nucleating particles that impact clouds and climate: Observational and modeling research needs. *Reviews of Geophysics*, *60*(2). https://doi.org/10.1029/2021rg000745

Canzi, A., Freney, E., Grzegorczyk, P., Baray, J.-L., & Planche, C. (2024). Characterization and parameterization of INP concentration variability regarding the source emissions origin [Dataset]. *OPGC, LaMP*. https://doi.org/10.25519/SH8R-F866

Chen, J., Wu, Z., Augustin-Bauditz, S., Grawe, S., Hartmann, M., Pei, X., et al. (2018). Ice-nucleating particle concentrations unaffected by urban air pollution in Beijing, China. *Atmospheric Chemistry and Physics*, *18*(5), 3523–3539. https://doi.org/10.5194/acp-18-3523-2018

Chen, J., Wu, Z., Gong, X., Qiu, Y., Chen, S., Zeng, L., & Hu, M. (2024). Anthropogenic dust as a significant source of Ice-Nucleating particles in the urban environment. *Earth's Future*, *12*(1). https://doi.org/10.1029/2023ef003738

Coen, M. C., Weingärtner, E., Apituley, A., Čeburnis, D., Fierz-Schmidhauser, R., Flentje, H., et al. (2010). Minimizing light absorption measurement artifacts of the Aethalometer: Evaluation of five correction algorithms. *Atmospheric Measurement Techniques*, *3*(2), 457–474. https://doi.org/10.5194/amt-3-457-2010

Creamean, J. M., Suski, K. J., Rosenfeld, D., Cazorla, A., DeMott, P. J., Sullivan, R. C., et al. (2013). Dust and biological aerosols from the Sahara and asia influence precipitation in the western U.S. *Science*, *339*(6127), 1572–1578. https://doi.org/10.1126/science.1227279

Cuesta-Mosquera, A., Glojek, K., Močnik, G., Drinovec, L., Gregorič, A., Rigler, M., et al. (2024). Optical properties and simple forcing efficiency of the organic aerosols and black carbon emitted by residential wood burning in rural central Europe. *Atmospheric Chemistry and Physics*, *24*(4), 2583–2605. https://doi.org/10.5194/acp-24-2583-2024

Cziczo, D. J., Ladino, L., Boose, Y., Kanji, Z. A., Kupiszewski, P., Lance, S., et al. (2017). Measurements of ice nucleating particles and ice residuals. *Meteorological Monographs*, *58*, 8.1–8.13. https://doi.org/10.1175/amsmonographs-d-16-0008.1

Deguillaume, L., Charbouillot, T., Joly, M., Vaïtilingom, M., Parazols, M., Marinoni, A., et al. (2014). Classification of clouds sampled at the puy de Dôme (France) based on 10 yr of monitoring of their physicochemical properties. *Atmospheric Chemistry and Physics*, *14*(3), 1485–1506. https://doi.org/10.5194/acp-14-1485-2014

DeMott, P. J., Hill, T. C. J., McCluskey, C. S., Prather, K. A., Collins, D. B., Sullivan, R. C., et al. (2016). Sea spray aerosol as a unique source of ice nucleating particles. *Proceedings of the National Academy of Sciences of the United States of America*, *113*(21), 5797–5803. https://doi.org/10.1073/pnas.1514034112

DeMott, P. J., Hill, T. C. J., Petters, M. D., Bertram, A. K., Tobo, Y., Mason, R. H., et al. (2017). Comparative measurements of ambient atmospheric concentrations of ice nucleating particles using multiple immersion freezing methods and a continuous flow diffusion chamber. *Atmospheric Chemistry and Physics*, *17*(18), 11227–11245. https://doi.org/10.5194/acp-17-11227-2017

DeMott, P. J., Möhler, O., Stetzer, O., Vali, G., Levin, Z., Petters, M. D., et al. (2011). Resurgence in ice nuclei measurement research. *Bulletin of the American Meteorological Society*, *92*(12), 1623–1635. https://doi.org/10.1175/2011bams3119.1

DeMott, P. J., Prenni, A. J., Liu, X., Kreidenweis, S. M., Petters, M. D., Twohy, C. H., et al. (2010). Predicting global atmospheric ice nuclei distributions and their impacts on climate. *Proceedings of the National Academy of Sciences of the United States of America*, *107*(25), 11217–11222. https://doi.org/10.1073/pnas.0910818107

DeMott, P. J., Prenni, A. J., McMeeking, G. R., Sullivan, R. C., Petters, M. D., Tobo, Y., et al. (2015). Integrating laboratory and field data to quantify the immersion freezing ice nucleation activity of mineral dust particles. *Atmospheric Chemistry and Physics*, *15*(1), 393–409. https://doi.org/10.5194/acp-15-393-2015

Denjean, C., Formenti, P., Desboeufs, K., Chevaillier, S., Triquet, S., Maillé, M., et al. (2016). Size distribution and optical properties of African mineral dust after intercontinental transport. *Journal of Geophysical Research: Atmospheres*, *121*(12), 7117–7138. https://doi.org/10.1002/2016jd024783

Fan, J., Leung, L. R., Rosenfeld, D., & DeMott, P. J. (2017). Effects of cloud condensation nuclei and ice nucleating particles on precipitation processes and supercooled liquid in mixed-phase orographic clouds. *Atmospheric Chemistry and Physics*, *17*(2), 1017–1035. https://doi.org/10.5194/acp-17-1017-2017

Farah, A., Freney, E., Canonaco, F., Prévôt, A. S. H., Pichon, J. M., Abboud, M., et al. (2021). Altitude aerosol measurements in Central France: Seasonality, sources and free-troposphere/boundary layer segregation. *Earth and Space Science*, *8*(3). https://doi.org/10.1029/2019ea001018

Farah, A., Freney, E., Chauvigne, A., Baray, J., Rose, C., Picard, D., et al. (2018). Seasonal Variation of Aerosol Size Distribution Data at the Puy de Dôme Station with Emphasis on the Boundary Layer/Free Troposphere Segregation. *Atmosphere*, *9*(7), 244. https://doi.org/10.3390/atmos9070244

Fialho, P., Hansen, A. D. A., & Honrath, R. E. (2005). Absorption coefficients by aerosols in remote areas: A new approach to decouple dust and black carbon absorption coefficients using seven-wavelength Aethalometer data. *Journal of Aerosol Science*, *36*(2), 267–282. https://doi.org/10.1016/j.jaerosci.2004.09.004

Flossmann, A. I., & Wobrock, W. (2010). A review of our understanding of the aerosol–cloud interaction from the perspective of a bin resolved cloud scale modelling. *Atmospheric Research*, *97*(4), 478–497. https://doi.org/10.1016/j.atmosres.2010.05.008

Freney, E., Sellegri, K., Asmi, E., Clemence, R., Chauvigné, A., Baray, J., et al. (2016). Experimental evidence of the feeding of the free troposphere with aerosol particles from the mixing layer. *Aerosol and Air Quality Research*, *16*(3), 702–716. https://doi.org/10.4209/aaqr.2015.03.0164

Freney, E., Sellegri, K., Canonaco, F., Boulon, J., Hervo, M., Weigel, R., et al. (2011). Seasonal variations in aerosol particle composition at the puy-de-Dôme research station in France. *Atmospheric Chemistry and Physics*, *11*(24), 13047–13059. https://doi.org/10.5194/acp-11-13047-2011

Fréville, P., Montoux, N., Baray, J., Chauvigne, A., Réverêt, F., Hervo, M., et al. (2015). LIDAR developments at Clermont-Ferrand—France for atmospheric observation. *Sensors*, *15*(2), 3041–3069. https://doi.org/10.3390/s150203041

Hoose, C., & Möhler, O. (2012). Heterogeneous ice nucleation on atmospheric aerosols: A review of results from laboratory experiments. *Atmospheric Chemistry and Physics*, *12*(20), 9817–9854. https://doi.org/10.5194/acp-12-9817-2012

Jahn, L. G., Polen, M. J., Jahl, L. G., Brubaker, T. A., Somers, J., & Sullivan, R. C. (2020). Biomass combustion produces ice-active minerals in biomass-burning aerosol and bottom ash. *Proceedings of the National Academy of Sciences of the United States of America*, *117*(36), 21928–21937. https://doi.org/10.1073/pnas.1922128117

Kanji, Z. A., Ladino, L. A., Wex, H., Boose, Y., Burkert-Kohn, M., Cziczo, D. J., & Krämer, M. (2017). Overview of Ice nucleating particles. *Meteorological Monographs*, *58*, 1.1–1.33. https://doi.org/10.1175/amsmonographs-d-16-0006.1

Kanji, Z. A., Welti, A., Corbin, J. C., & Mensah, A. A. (2020). Black carbon particles do not matter for immersion mode ice nucleation. *Geophysical Research Letters*, *47*(11). https://doi.org/10.1029/2019gl086764

Keita, S. A., Girard, E., Raut, J., Pelon, J., Blanchet, J., Lemoine, O., & Onishi, T. (2019). Simulating Arctic ice clouds during spring using an advanced ice cloud microphysics in the WRF model. *Atmosphere*, *10*(8), 433. https://doi.org/10.3390/atmos10080433

Lac, C., Chaboureau, J., Masson, V., Pinty, J. P., Tulet, P., Escobar, J. J., et al. (2018). Overview of the Meso-NH model version 5.4 and its applications. *Geoscientific Model Development*, *11*(5), 1929–1969. https://doi.org/10.5194/gmd-11-1929-2018

Lacher, L., Adams, M. P., Barry, K. R., Bertozzi, B., Bingemer, H., Boffo, C., et al. (2024). The Puy de Dôme ICe Nucleation Intercomparison Campaign (PICNIC): Comparison between online and offline methods in ambient air. *Atmospheric Chemistry and Physics*, *24*(4), 2651–2678. https://doi.org/10.5194/acp-24-2651-2024

Lacher, L., Clemen, H., Shen, X., Mertes, S., Gysel, M., Moallemi, A., et al. (2021). Sources and nature of ice-nucleating particles in the free troposphere at Jungfraujoch in winter 2017. *Atmospheric Chemistry and Physics*, *21*(22), 16925–16953. https://doi.org/10.5194/acp-21-16925-2021

Lacher, L., Lohmann, U., Boose, Y., Zipori, A., Herrmann, E., Bukowiecki, N., et al. (2017). The Horizontal Ice Nucleation Chamber (HINC): INP measurements at conditions relevant for mixed-phase clouds at the High Altitude Research Station Jungfraujoch. *Atmospheric Chemistry and Physics*, *17*(24), 15199–15224. https://doi.org/10.5194/acp-17-15199-2017

Lafon, S., Sokolik, I. N., Rajot, J., Caquineau, S., & Gaudichet, A. (2006). Characterization of iron oxides in mineral dust aerosols: Implications for light absorption. *Journal of Geophysical Research*, *111*(D21). https://doi.org/10.1029/2005jd007016

Levin, E. J. T., McMeeking, G. R., DeMott, P. J., McCluskey, C. S., Carrico, C. M., Nakao, S., et al. (2016). Ice-nucleating particle emissions from biomass combustion and the potential importance of soot aerosol. *Journal of Geophysical Research: Atmospheres*, *121*(10), 5888–5903. https://doi.org/10.1002/2016jd024879

Mahrt, F., Marcolli, C., David, R. O., Grönquist, P., Meier, E. J. B., Lohmann, U., & Kanji, Z. A. (2018). Ice nucleation abilities of soot particles determined with the Horizontal Ice Nucleation Chamber. *Atmospheric Chemistry and Physics*, *18*(18), 13363–13392. https://doi.org/10.5194/acp-18-13363-2018

Mahrt, F., Rösch, C., Gao, K., Dreimol, C. H., Zawadowicz, M. A., & Kanji, Z. A. (2023). Physicochemical properties of charcoal aerosols derived from biomass pyrolysis affect their ice-nucleating abilities at cirrus and mixed-phase cloud conditions. *Atmospheric Chemistry and Physics*, *23*(2), 1285–1308. https://doi.org/10.5194/acp-23-1285-2023

Mann, G. W., Carslaw, K. S., Spracklen, D. V., Ridley, D. A., Manktelow, P. T., Chipperfield, M. P., et al. (2010). Description and evaluation of GLOMAP-mode: A modal global aerosol microphysics model for the UKCA composition-climate model. *Geoscientific Model Development*, *3*(2), 519–551. https://doi.org/10.5194/gmd-3-519-2010

Marécal, V., Peuch, V., Andersson, C., Andersson, S., Arteta, J., Beekmann, M., et al. (2015). A regional air quality forecasting system over Europe: The MACC-II daily ensemble production. *Geoscientific Model Development*, *8*(9), 2777–2813. https://doi.org/10.5194/gmd-8-2777-2015

Mason, R. H., Si, M., Li, J., Chou, C., Dickie, R., Toom-Sauntry, D., et al. (2015). Ice nucleating particles at a coastal marine boundary layer site: Correlations with aerosol type and meteorological conditions. *Atmospheric Chemistry and Physics*, *15*(21), 12547–12566. https://doi.org/10.5194/acp-15-12547-2015

McCluskey, C. S., DeMott, P. J., Prenni, A. J., Levin, E. J. T., McMeeking, G. R., Sullivan, A. P., et al. (2014). Characteristics of atmospheric ice nucleating particles associated with biomass burning in the US: Prescribed burns and wildfires. *Journal of Geophysical Research: Atmospheres*, *119*(17), 10458–10470. https://doi.org/10.1002/2014jd021980

McCluskey, C. S., Ovadnevaitė, J., Rinaldi, M., Atkinson, J., Belosi, F., Čeburnis, D., et al. (2018). Marine and terrestrial organic Ice-Nucleating particles in pristine marine to continentally influenced northeast Atlantic air masses. *Journal of Geophysical Research: Atmospheres*, *123*(11), 6196–6212. https://doi.org/10.1029/2017jd028033

Meyers, M. P., DeMott, P. J., & Cotton, W. R. (1992). New primary ice-nucleation parameterizations in an explicit cloud model. *Journal of Applied Meteorology and Climatology*, *31*(7), 708–721. https://doi.org/10.1175/1520-0450(1992)031<0708:NPINPI>2.0.CO;2

Milbrandt, J. A., & Yau, M. K. (2005). A Multimoment bulk Microphysics Parameterization. Part I: Analysis of the role of the spectral shape parameter. *Journal of the Atmospheric Sciences*, *62*(9), 3051–3064. https://doi.org/10.1175/jas3534.1

Möhler, O., Adams, M. P., Lacher, L., Vogel, F., Nadolny, J., Ullrich, R., et al. (2021). The Portable Ice Nucleation Experiment (PINE): A new online instrument for laboratory studies and automated long-term field observations of ice-nucleating particles. *Atmospheric Measurement Techniques*, *14*(2), 1143–1166. https://doi.org/10.5194/amt-14-1143-2021

Möhler, O., Field, P. R., Connolly, P., Benz, S., Saathoff, H., Schnaiter, M., et al. (2006). Efficiency of the deposition mode ice nucleation on mineral dust particles. *Atmospheric Chemistry and Physics*, *6*(10), 3007–3021. https://doi.org/10.5194/acp-6-3007-2006

Muhlbauer, A., & Lohmann, U. (2009). Sensitivity studies of aerosol–cloud interactions in mixed-phase orographic precipitation. *Journal of the Atmospheric Sciences*, *66*(9), 2517–2538. https://doi.org/10.1175/2009jas3001.1

Müller, T., Henzing, B., De Leeuw, G., Wiedensohler, A., Alastuey, A., Angelov, H., et al. (2011). Characterization and intercomparison of aerosol absorption photometers: Result of two intercomparison workshops. *Atmospheric Measurement Techniques*, *4*(2), 245–268. https://doi.org/10.5194/amt-4-245-2011

Niemand, M., Möhler, O., Vogel, B., Vogel, H., Hoose, C., Connolly, P., et al. (2012). A Particle-Surface-Area-Based parameterization of immersion freezing on desert dust particles. *Journal of the Atmospheric Sciences*, *69*(10), 3077–3092. https://doi.org/10.1175/jas-d-11-0249.1

O'Sullivan, D., Murray, B. J., Malkin, T. L., Whale, T. F., Umo, N. S., Atkinson, J. D., et al. (2014). Ice nucleation by fertile soil dusts: Relative importance of mineral and biogenic components. *Atmospheric Chemistry and Physics*, *14*(4), 1853–1867. https://doi.org/10.5194/acp-14-1853-2014

Petzold, A., Schloesser, H., Sheridan, P. J., Arnott, W. P., Ogren, J. A., & Virkkula, A. (2005). Evaluation of multiangle absorption photometry for measuring aerosol light absorption. *Aerosol Science and Technology*, *39*(1), 40–51. https://doi.org/10.1080/027868290901945

Petzold, A., & Schönlinner, M. (2004). Multi-angle absorption photometry—A new method for the measurement of aerosol light absorption and atmospheric black carbon. *Journal of Aerosol Science*, *35*(4), 421–441. https://doi.org/10.1016/j.jaerosci.2003.09.005

Phillips, V. T. J., DeMott, P. J., & Andronache, C. (2008). An empirical parameterization of heterogeneous ice nucleation for multiple chemical species of aerosol. *Journal of the Atmospheric Sciences*, *65*(9), 2757–2783. https://doi.org/10.1175/2007jas2546.1

Planche, C., Mann, G. W., Carslaw, K. S., Dalvi, M., Marsham, J. H., & Field, P. R. (2017). Spatial and temporal CCN variations in convection-permitting aerosol microphysics simulations in an idealised marine tropical domain. *Atmospheric Chemistry and Physics*, *17*(5), 3371–3384. https://doi.org/10.5194/acp-17-3371-2017

Planche, C., Marsham, J. H., Field, P. R., Carslaw, K. S., Hill, A. A., Mann, G. W., & Shipway, B. J. (2015). Precipitation sensitivity to auto-conversion rate in a numerical weather-prediction model. *Quarterly Journal of the Royal Meteorological Society*, *141*(691), 2032–2044. https://doi.org/10.1002/qj.2497

Planche, C., Wobrock, W., & Flossmann, A. I. (2014). The continuous melting process in a cloud-scale model using a bin microphysics scheme. *Quarterly Journal of the Royal Meteorological Society*, *140*(683), 1986–1996. https://doi.org/10.1002/qj.2265

Planche, C., Wobrock, W., Flossmann, A. I., Tridon, F., Van Baelen, J., Pointin, Y., & Hagen, M. (2010). The influence of aerosol particle number and hygroscopicity on the evolution of convective cloud systems and their precipitation: A numerical study based on the COPS observations on 12 August 2007. *Atmospheric Research*, *98*(1), 40–56. https://doi.org/10.1016/j.atmosres.2010.05.003

Prenni, A. J., Demott, P. J., Rogers, D. C., Kreidenweis, S. M., Mcfarquhar, G. M., Zhang, G., & Poellot, M. R. (2009). Ice nuclei characteristics from M-PACE and their relation to ice formation in clouds. *Tellus B: Chemical and Physical Meteorology*, *61*(2), 436–448. https://doi.org/10.1111/j.1600-0889.2009.00415.x

Pruppacher, H. R., & Klett, J. D. (1997). *Microphysics of clouds and precipitation* (p. 954). Kluwer Academic.

Ren, Y. Z., Bi, K., Fu, S. Z., Tian, P., Huang, M. Y., Zhu, R. H., & Xue, H. W. (2023). The relationship of aerosol properties and Ice-Nucleating particle concentrations in Beijing. *Journal of Geophysical Research: Atmospheres*, *128*(10). https://doi.org/10.1029/2022jd037383

Rogers, D. C. (1993). Measurements of natural ice nuclei with a continuous flow diffusion chamber. *Atmospheric Research*, *29*(3–4), 209–228. https://doi.org/10.1016/0169-8095(93)90004-8

Rogers, D. C., DeMott, P. J., Kreidenweis, S. M., & Chen, Y. (2001). A continuous-flow diffusion chamber for airborne measurements of ice nuclei. *Journal of Atmospheric and Oceanic Technology*, *18*(5), 725–741. https://doi.org/10.1175/1520-0426(2001)018<0725:ACFDCF>2.0.CO;2

Schmidt, L., Schäfer, D., Geller, J., Lünenschloss, P., Palm, B., Rinke, K., et al. (2023). System for automated Quality Control (SaQC) to enable traceable and reproducible data streams in environmental science. *Environmental Modelling and Software*, *169*, 105809. ISSN 1364-8152. https://doi.org/10.1016/j.envsoft.2023.105809

Schneider, J., Höhler, K., Heikkilä, P., Keskinen, J., Bertozzi, B., Bogert, P., et al. (2021). The seasonal cycle of ice-nucleating particles linked to the abundance of biogenic aerosol in boreal forests. *Atmospheric Chemistry and Physics*, *21*(5), 3899–3918. https://doi.org/10.5194/acp-21-3899-2021

Skamarock, W. C., Klemp, J., Dudhia, J., Gill, D. O., Barker, D., Wang, W., & Powers, J. G. (2008). A description of the advanced research WRF version 3. 27 (pp. 3–27).

Steinke, I., Funk, R., Busse, J., Iturri, A., Kirchen, S., Leue, M., et al. (2016). Ice nucleation activity of agricultural soil dust aerosols from Mongolia, Argentina, and Germany. *Journal of Geophysical Research: Atmospheres*, *121*(22). https://doi.org/10.1002/2016jd025160

Steinke, I., Hoose, C., Möhler, O., Connolly, P., & Leisner, T. (2015). A new temperature- and humidity-dependent surface site density approach for deposition ice nucleation. *Atmospheric Chemistry and Physics*, *15*(7), 3703–3717. https://doi.org/10.5194/acp-15-3703-2015

Suski, K. J., Hill, T. C. J., Levin, E. J. T., Miller, A., DeMott, P. J., & Kreidenweis, S. M. (2018). Agricultural harvesting emissions of ice-nucleating particles. *Atmospheric Chemistry and Physics*, *18*(18), 13755–13771. https://doi.org/10.5194/acp-18-13755-2018

Tan, I., & Storelvmo, T. (2016). Sensitivity study on the influence of cloud microphysical parameters on mixed-phase cloud thermodynamic phase partitioning in CAM5. *Journal of the Atmospheric Sciences*, *73*(2), 709–728. https://doi.org/10.1175/jas-d-15-0152.1

Tetens, O. (1930). Uber einige meteorologische Begriffe. *Zeitschrift für Geophysik*, *6*, 297–309.

Tinorua, S., Denjean, C., Nabat, P., Pont, V., Arnaud, M., Bourrianne, T., et al. (2024). Two-year intercomparison of three methods for measuring black carbon concentration at a high-altitude research station in Europe. *EGUsphere*. https://doi.org/10.5194/egusphere-2024-47

Tobo, Y., DeMott, P. J., Hill, T. C. J., Prenni, A. J., Swoboda-Colberg, N. G., Franc, G. D., & Kreidenweis, S. M. (2014). Organic matter matters for ice nuclei of agricultural soil origin. *Atmospheric Chemistry and Physics*, *14*(16), 8521–8531. https://doi.org/10.5194/acp-14-8521-2014

Trueblood, J. V., Nicosia, A., Engel, A., Zäncker, B., Rinaldi, M., Freney, E., et al. (2021). A two-component parameterization of marine ice-nucleating particles based on seawater biology and sea spray aerosol measurements in the Mediterranean Sea. *Atmospheric Chemistry and Physics*, *21*(6), 4659–4676. https://doi.org/10.5194/acp-21-4659-2021

Vali, G., DeMott, P. J., Möhler, O., & Whale, T. F. (2015). Technical note: A proposal for ice nucleation terminology. *Atmospheric Chemistry and Physics*, *15*(18), 10263–10270. https://doi.org/10.5194/acp-15-10263-2015

Venzac, H., Sellegri, K., Villani, P., Picard, D., & Laj, P. (2009). Seasonal variation of aerosol size distributions in the free troposphere and residual layer at the puy de Dôme station, France. *Atmospheric Chemistry and Physics*, *9*(4), 1465–1478. https://doi.org/10.5194/acp-9-1465-2009

Vergara-Temprado, J., Miltenberger, A. K., Furtado, K., Grosvenor, D. P., Shipway, B. J., Hill, A. A., et al. (2018). Strong control of Southern Ocean cloud reflectivity by ice-nucleating particles. *Proceedings of the National Academy of Sciences of the United States of America*, *115*(11), 2687–2692. https://doi.org/10.1073/pnas.1721627115

Vergara-Temprado, J., Murray, B. J., Wilson, T. W., O'Sullivan, D., Browse, J., Pringle, K. J., et al. (2017). Contribution of feldspar and marine organic aerosols to global ice nucleating particle concentrations. *Atmospheric Chemistry and Physics*, *17*(5), 3637–3658. https://doi.org/10.5194/acp-17-3637-2017

Vié, B., Pinty, J. P., Berthet, S., & Leriche, M. (2016). LIMA (v1.0): A quasi two-moment microphysical scheme driven by a multimodal population of cloud condensation and ice freezing nuclei. *Geoscientific Model Development*, *9*(2), 567–586. https://doi.org/10.5194/gmd-9-567-2016

Vogel, F., Adams, M. P., Lacher, L., Foster, P. B., Porter, G. C. E., Bertozzi, B., et al. (2024). Ice-nucleating particles active below −24°C in a Finnish boreal forest and their relationship to bioaerosols. *Atmospheric Chemistry and Physics*, *24*(20), 11737–11757. https://doi.org/10.5194/acp-24-11737-2024

Wilbourn, E. K., Lacher, L., Guerrero, C., Vepuri, H. S. K., Höhler, K., Nadolny, J., et al. (2024). Measurement report: A comparison of ground-level ice-nucleating-particle abundance and aerosol properties during autumn at contrasting marine and terrestrial locations. *Atmospheric Chemistry and Physics*, *24*(9), 5433–5456. https://doi.org/10.5194/acp-24-5433-2024

Willeke, K., & Baron, P. (2005). *Aerosol measurement: Principles, techniques, and applications*. Van Nostrand Reinhold.

Wilson, T. W., Ladino, L. A., Alpert, P. A., Breckels, M. N., Brooks, I. M., Browse, J., et al. (2015). A marine biogenic source of atmospheric ice-nucleating particles. *Nature*, *525*(7568), 234–238. https://doi.org/10.1038/nature14986

Zhao, B., Wang, Y., Gu, Y., Liou, K., Jiang, J. H., Fan, J., et al. (2019). Ice nucleation by aerosols from anthropogenic pollution. *Nature Geoscience*, *12*(8), 602–607. https://doi.org/10.1038/s41561-019-0389-4